

Quantum optics of strongly laser-driven atoms and generation of high photon number optical cat states

J. Rivera-Dean,¹ Th. Lamprou,^{2,3} E. Pisanty,^{1,4} P. Stammer,^{1,4} A. F. Ordóñez,¹ M. F. Ciappina,^{1,5,6} M. Lewenstein,^{1,7,*} and P. Tzallas^{2,8,†}

¹*ICFO – Institut de Ciències Fotoniques, The Barcelona Institute of Science and Technology, 08860 Castelldefels (Barcelona)*

²*Foundation for Research and Technology-Hellas,*

Institute of Electronic Structure & Laser, GR-70013 Heraklion (Crete), Greece

³*Department of Physics, University of Crete, P.O. Box 2208, GR-71003 Heraklion (Crete), Greece*

⁴*Max Born Institute for Nonlinear Optics and Short Pulse Spectroscopy,
Max Born Strasse 2a, D-12489 Berlin, Germany*

⁵*Physics Program, Guangdong Technion - Israel Institute of Technology,
241 Daxue Road, Shantou, Guangdong, China, 515063*

⁶*Technion – Israel Institute of Technology, Haifa, 32000, Israel*

⁷*ICREA, Pg. Lluís Companys 23, 08010 Barcelona, Spain*

⁸*ELI-ALPS, ELI-Hu Non-Profit Ltd., Dugonics tér 13, H-6720 Szeged, Hungary*

(Dated: June 6, 2022)

Recently we have demonstrated the quantum nature of light in strongly laser driven atoms, and we have shown how the process of high harmonic generation can be used for the creation of highly non-classical light states, in particular superpositions of two coherent states, i.e., optical Schrödinger “cat” states [M. Lewenstein et al., *Generation of optical Schrödinger cat states in intense laser-matter interactions*, Nat. Phys. (2021)]. Here, we investigate the quantum optical description of the interaction, incorporating many atoms and the back-action of the high harmonic generation or above threshold ionization processes on the coherent state of the driving laser field. We show how the conditioning on high harmonic generation and above threshold ionization can lead to non-classical light states, and we discuss the key parameters that can be used for controlling and characterizing the non-classical states obtained after high harmonic generation. The theoretical results have been experimentally confirmed by demonstrating how the obtained coherent state superposition transitions from an optical “cat” to “kitten” state by changing the number of atoms participating in the high harmonic generation process. Additionally, we experimentally verify the applicability of the approach for generating high photon number non-classical light states. This is shown by demonstrating the generation of a 9-photon optical “cat” state which, to our knowledge, is the highest photon number optical “cat” state experimentally reported. Our findings anticipate the development of new methods that naturally lead to the creation of high photon number controllable coherent state superpositions, advancing investigations in quantum technology.

I. INTRODUCTION

The interaction of atoms with intense laser fields is at the center of interest in atomic, molecular and optical physics since the development of high power pulsed laser sources. It has been used for the generation of coherent radiation in the extreme ultraviolet (XUV) [1–7] and X-rays [8, 9], and has been substantially applied in attosecond science [7, 10, 11], non-linear XUV optics [12–19], high resolution spectroscopy [20, 21] and tomography [22, 23]. The qualitative understanding of the interaction is traditionally provided by the well known three-step model [24–26]. According to this model, when a low frequency (usually in the infrared (IR) spectral range) intense linearly polarized laser field interacts with an atom or molecule, an electron tunnels out from the considered system, then it accelerates in the continuum gaining energy from the laser field and, within the same cycle of

the field, it may re-collide elastically or inelastically with the parent ion. This process is repeated every half cycle of the laser field leading to the generation of ions, photoelectrons or photons with frequencies higher than the driving laser field (high harmonics (HH)). The non-recolliding electrons and the electrons that re-collide elastically with the parent ion contribute to the generation of Above Threshold Ionization (ATI) photoelectrons [3, 27], while the inelastic recollision leads to the generation of HH (electron recombines with the ion emitting a photon) or multiple charged ions (for example, via non-sequential double ionization) [3]. Due to the high photon number of the driving field, this model employs semi-classical approximations treating the electromagnetic field classically and the electron quantum mechanically. The success of the classical treatment of the electromagnetic field suggested no need to consider the quantum aspects of the field thus far, leaving unexploited advantages emerging from the connection between quantum optics [28–32] and strong laser-field physics [33, 34].

To overcome this barrier we have to provide an answer to the question “*what is the quantum depletion of the fundamental laser mode and the quantum state of the*

* maciej.lewenstein@icfo.eu

† ptzallas@iesl.forth.gr

light field (fundamental and harmonics) after the interaction?" underlying the majority of experiments using intense laser-atom interactions. Several groups attempted to introduce fully quantized theoretical approaches for the description of intense laser-atom interactions [35–49]. However, despite the important information obtained from these studies, none of them provides a rigorous answer to the above question. This is because either they are devoted on investigating the properties of the interaction products (harmonic photons, electrons, ions) without taking into account the back-action of the interaction on the quantum state of the driving field or, if they do, they rely on simplified two-level systems. Also, the recently developed theoretical [50] and experimental [51] investigations addressing this matter do not provide information about the character of the quantum state of the light field after the interaction. A rigorous answer to the above question was recently reported in ref. [52], by demonstrating theoretically and experimentally the quantum nature of light in intense laser-atom interactions. Upon conditioning on high harmonic generation (HHG) process, one obtains in effect highly non-classical light states. Experimentally, this was achieved by combining the Quantum Tomography (QT) [53, 54] with the Quantum Spectrometer (QS) [51, 55] approach. It was shown that: I) when an atomic ensemble interacts with a driving laser in a coherent state $|\alpha_L\rangle$, the quantum state of the driving field and of the harmonics after the interaction are coherent, with the fundamental mode to be shifted by $|\alpha_L\rangle \rightarrow |\alpha_L + \delta\alpha_L\rangle$; II) the final state of the fundamental mode, conditioned on harmonic generation, is an optical Schrödinger “cat” state resulting from the superposition of the initial and the shifted coherent states. These results open the path for further investigations towards the generation of arbitrary high photon number coherent state superpositions, and the control of their quantum features by changing the intense laser-atom interaction conditions and/or by utilizing conditioning approaches on processes other than HHG, such as ATI.

Towards this direction, here we investigate the quantum optics of intense laser-atom interactions. Specifically, we study HHG and ATI processes and their back-action $\delta\alpha_L$ on the coherent state of the driving field. We analyze the phase space dynamics of $\delta\alpha_L$ within one cycle of the field and along the duration of the driving pulse envelope, and show how the key action of conditioning on HHG and ATI processes can naturally lead to the generation of coherent state superpositions of arbitrary high photon number. We also discuss how the laser-atom interaction conditions, via $\delta\alpha_L$, can be used to control the quantum features of these states. The theoretical results have been confirmed experimentally by showing the dependence of the non-classical features of the generated light after HHG on the atomic gas pressure. Furthermore, to demonstrate the high photon nature of the generated cat states, we have experimentally achieved a 9-photon optical cat state.

The numerical implementation employed for performing the theoretical calculations and their corresponding plots are made available in [56].

II. QUANTUM OPTICS: THEORETICAL APPROACH

Our starting point is the time-dependent Schrödinger equation (TDSE) describing the interaction of the quantized electromagnetic field with a single electron

$$i\hbar \frac{\partial}{\partial t} |\tilde{\Psi}(t)\rangle = \hat{H}(t) |\tilde{\Psi}(t)\rangle, \quad (1)$$

where

$$\hat{H}(t) = \hat{H}_0 + \hat{H}_I + \hat{H}_f. \quad (2)$$

Here, $\hat{H}_0 = \hat{\mathbf{P}}^2/2m + V(\hat{\mathbf{R}})$ is the Hamiltonian describing the electron bound to a potential $V(\hat{\mathbf{R}})$, $\hat{H}_I = -e\hat{\mathbf{E}} \cdot \hat{\mathbf{R}}$ is the dipole coupling that introduces the interaction between the electron and the field in the dipole approximation, and \hat{H}_f is the electromagnetic free-field Hamiltonian. In the following, we will represent the electronic quadrature operators with capital letters (\hat{X}, \hat{P}), while the photonic ones with lower-case letters (\hat{x}, \hat{p}).

As we aim to describe laser/harmonic pulses of finite duration, we should consider in the free-field term \hat{H}_f the full continuum spectrum of the electromagnetic field. Nevertheless, for the sake of simplicity, we write it as the sum of effective discrete modes containing the one obtained from the laser with frequency ω_L and its harmonics of frequencies $\omega_q = q\omega_L$, with $q = 1, 2, 3, \dots$ up to the cut-off region of the spectrum. Concretely, we have

$$\hat{H}_f = \hbar\omega_L \hat{a}^\dagger \hat{a} + \sum_{q=2}^{\text{cutoff}} \hbar q\omega_L \hat{b}_q^\dagger \hat{b}_q, \quad (3)$$

where \hat{a}^\dagger (\hat{a}) and \hat{b}_q^\dagger (\hat{b}_q) are the creation (annihilation) operators acting over the laser and the q th harmonic mode, respectively. Following the same idea, we model the laser electric field operator as

$$\hat{\mathbf{E}}(t) = -i\hbar\mathbf{g}(\omega_L)f(t) \left[(\hat{a}^\dagger - \hat{a}) + \sum_{q=2}^{\text{cutoff}} \sqrt{q}(\hat{b}_q^\dagger - \hat{b}_q) \right]. \quad (4)$$

Here, we denote by $\mathbf{g}(\omega_L) \propto \sqrt{\omega_L/V_{\text{eff}}}$ the coefficient that enters into the expansion of the laser electric field modes and that depends on V_{eff} , which is the effective quantization volume [57, 58]. Thus, $\mathbf{e}\mathbf{g}(\omega_L)$ encodes information about the polarization modes and has dimensions [$\text{m}^{-1}\text{s}^{-1}$]. Finally, $0 \leq f(t) \leq 1$ is a dimensionless function describing the pulse envelope.

At time $t = t_0$, we can describe the state of the system by $|\Psi(t_0)\rangle = |g, \alpha_L, \Omega_H\rangle$, that is, with the electron lying on the atomic ground state, the laser mode in a coherent state and the harmonic modes in the vacuum

state. Within this context, the first transformation we apply consists of moving to the interaction picture with respect to the electromagnetic field \hat{H}_f , i.e.,

$$|\tilde{\Psi}(t)\rangle = \exp[-i\hat{H}_f t] |\Psi'(t)\rangle, \quad (5)$$

so that Eq. (1) reads

$$i\hbar \frac{\partial}{\partial t} |\Psi'(t)\rangle = [\hat{H}_0 - e\hat{\mathbf{E}}(t) \cdot \hat{\mathbf{R}}] |\Psi'(t)\rangle, \quad (6)$$

where the laser electric field operator defined in Eq. (4) has an extra time dependence

$$\begin{aligned} \hat{\mathbf{E}}(t) = & -i\hbar \mathbf{g}(\omega_L) f(t) \left[(\hat{a}^\dagger e^{i\omega_L t} - \hat{a} e^{-i\omega_L t}) \right. \\ & \left. + \sum_{q=2}^{\text{cutoff}} \sqrt{q} (\hat{b}_q^\dagger e^{iq\omega_L t} - \hat{b}_q e^{-iq\omega_L t}) \right]. \end{aligned} \quad (7)$$

The second transformation we apply consists of a displacement in the subspace of the driving laser field of a quantity α_L , i.e.,

$$|\Psi'(t)\rangle = \hat{D}(\alpha_L) |\Psi(t)\rangle, \quad (8)$$

where $\hat{D}(\alpha_L)$ is the optical displacement operator [58], acting over the laser mode. Recalling the following properties of this operator [59]

$$\hat{D}(\alpha)^\dagger \hat{D}(\alpha) = \mathbb{1}, \quad (9)$$

$$\hat{D}(\alpha) \hat{a} \hat{D}^\dagger(\alpha) = \hat{a} - \alpha, \quad (10)$$

its introduction in our equations has two mutually related consequences: it sets the initial state of the laser mode to a vacuum state Ω_L , and transforms our TDSE into

$$\begin{aligned} i\hbar \frac{\partial}{\partial t} |\Psi(t)\rangle = & \left[\hat{H}_0 - e\mathbf{E}_L(t) \cdot \hat{\mathbf{R}} - e\hat{\mathbf{E}}_Q(t) \cdot \hat{\mathbf{R}} \right] |\Psi(t)\rangle \\ = & \left[\hat{H}_{\text{sc}} - e\hat{\mathbf{E}}_Q(t) \cdot \hat{\mathbf{R}} \right] |\Psi(t)\rangle. \end{aligned} \quad (11)$$

Here, $\mathbf{E}_L(t)$ accounts for the classical electric field part of the laser pulse

$$\mathbf{E}_L(t) = -i\hbar \mathbf{g}(\omega_L) f(t) \left[\alpha_L^* e^{i\omega_L t} - \alpha_L e^{-i\omega_L t} \right], \quad (12)$$

so \hat{H}_{sc} represents the semiclassical part of our Hamiltonian [26]. On the other hand, $\hat{\mathbf{E}}_Q(t)$ is the quantum correction term defined as in Eq. (7).

Lastly, we move to the interaction picture with respect to the semiclassical Hamiltonian \hat{H}_{sc}

$$|\Psi(t)\rangle = \mathcal{T} \exp \left[-i \int_{t_0}^t dt' \hat{H}_{\text{sc}}(t') / \hbar \right] |\psi(t)\rangle, \quad (13)$$

where \mathcal{T} is the time-ordering operator. This last transformation leads us to the final form of our TDSE, which we will use throughout this manuscript, i.e.

$$i\hbar \frac{\partial}{\partial t} |\psi(t)\rangle = -e\hat{\mathbf{E}}_Q(t) \cdot \hat{\mathbf{R}}_H(t) |\psi(t)\rangle, \quad (14)$$

where $e\hat{\mathbf{R}}_H(t)$ denotes the time-dependent dipole operator in the considered semi-classical interaction picture, acting exclusively on the electronic degrees of freedom. This evolution drives the dynamics of the field and the electron, which we can find remaining in the ground state or in a continuum state. At the same time, we can hardly find it in some bound excited state.

A. Quantum optical description of HHG

In the HHG process, the electron gets first transferred to the continuum via tunneling ionization due to the strong laser field we are applying and, later on, it recombines with the parent ion that was left behind, ending up again in the ground state of the system. Therefore, in order to get information about the HHG photonic quantum state, we condition Eq. (14) onto the atomic ground state $|g\rangle$, i.e.,

$$i\hbar \frac{\partial}{\partial t} \langle g | \psi(t) \rangle = -\hat{\mathbf{E}}_Q(t) \cdot \langle g | e\hat{\mathbf{R}}_H(t) | \psi(t) \rangle. \quad (15)$$

Defining the identity operator as

$$\mathbb{1} = |g\rangle\langle g| + \sum_{\phi_b} |\phi_b\rangle\langle \phi_b| + \int d\phi_c |\phi_c\rangle\langle \phi_c|, \quad (16)$$

where we denote with the discrete sum the set of atomic bound excited states, and with the integral the set of continuum states, we introduce it in Eq. (15) to get

$$\begin{aligned} i\hbar \frac{\partial}{\partial t} \langle g | \psi(t) \rangle = & -\hat{\mathbf{E}}_Q(t) \cdot \left[\mathbf{d}_H(t) \langle g | \psi(t) \rangle \right. \\ & \left. + \sum_{\phi_b} \mathbf{d}_H(\phi_b, t) \langle \phi_b | \psi(t) \rangle \right. \\ & \left. + \int d\phi_c \mathbf{d}_H(\phi_c, t) \langle \phi_c | \psi(t) \rangle \right]. \end{aligned} \quad (17)$$

In this last expression, we denote with $\mathbf{d}_H(t) = \langle g | e\hat{\mathbf{R}}_H(t) | g \rangle$ the quantum averaged time-dependent dipole moment and with $\mathbf{d}_H(\phi_k, t) = \langle g | e\hat{\mathbf{R}}_H(t) | \phi_k \rangle$ the matrix element between the ground state and state $|\phi_k\rangle$, where k can take values b or c depending on whether the state belongs to the bound excited states or to the continuum region of the spectrum, respectively. Each of these terms is multiplied by the probability amplitude of finding the electron either in the ground state, in another excited bound state or in an excited continuum state. In the first attempt to solve the problem, we will assume that these two last terms are very small in comparison to the first one, which is a fair assumption as the electron hardly remains in an excited bound/continuum state [7, 26] at the end of the pulse. Therefore, our TDSE adopts the following form

$$i\hbar \frac{\partial}{\partial t} |\Phi(t)\rangle = -\hat{\mathbf{E}}_Q(t) \cdot \mathbf{d}_H(t) |\Phi(t)\rangle, \quad (18)$$

where $|\Phi(t)\rangle = \langle \mathbf{g} | \psi(t) \rangle$. Here, $\mathbf{d}_H(t)$ can be easily calculated by numerically solving the TDSE, or by means of the Strong Field Approximation (SFA) theory [7, 26, 60]. Whatever the method used, this equation can be easily solved as it is written as a linear combination of photon creation and annihilation operators for the different modes considered in the problem. This has a natural implication, and is that the final solution is given by a product state of all the modes participating in the process,

$$|\Phi(t)\rangle = |\Phi_{q=1}(t)\rangle \otimes |\Phi_{q=2}(t)\rangle \otimes \dots \otimes |\Phi_{q=\text{cutoff}}(t)\rangle, \quad (19)$$

so we can solve the equation for a given q and then generalize the result to the rest. Thus, the single mode version of Eq. (18) which we will now deal with is

$$\begin{aligned} i\hbar \frac{\partial}{\partial t} |\Phi_q(t)\rangle &= -\hat{\mathbf{E}}_q(t) \cdot \mathbf{d}_H(t) |\Phi(t)\rangle \\ &= \hat{H}_q(t) |\Phi(t)\rangle, \end{aligned} \quad (20)$$

where

$$\hat{\mathbf{E}}_q(t) = -i\hbar \mathbf{g}(\omega_L) f(t) \sqrt{q} \left[\hat{b}_q^\dagger e^{iq\omega_L t} - \hat{b}_q e^{-iq\omega_L t} \right]. \quad (21)$$

In general, we can write the solution to this equation as [61]

$$|\Phi_q(t)\rangle = \hat{U}_q(t, t_0) |\Phi_q(t_0)\rangle, \quad (22)$$

where $\hat{U}(t, t_0)$ is our time-evolution operator. Furthermore, we can split our time interval in N steps of size Δt , which is typically defined to be inversely proportional to N , such that we can write this operator as

$$\hat{U}_q(t, t_0) = \lim_{N \rightarrow \infty} \prod_{i=0}^{N-1} \hat{U}_q(t_{i+1}, t_i), \quad (23)$$

where we identify $t_N = t$. Therefore, we can write each of the unitary operators appearing in the previous product as

$$\hat{U}_q(t_{i+1}, t_i) = \exp \left[-i \hat{H}_q(t_{i+1}) \Delta t / \hbar \right]. \quad (24)$$

Let us take a closer look to the commutation relation between $\hat{H}_q(t)$ defined at two different times t and t'

$$\begin{aligned} i \left[\hat{H}_q(t), \hat{H}_q(t') \right] &= -2q\hbar^2 f(t) f(t') (\mathbf{g}(\omega_L) \cdot \mathbf{d}_H(t)) \\ &\quad \times (\mathbf{g}(\omega_L) \cdot \mathbf{d}_H(t')) \sin(q\omega_L(t - t')) \mathbb{1}. \end{aligned} \quad (25)$$

As we can see, this term is a function proportional to the identity operator, something that favours the implementation of the Baker-Campbell-Hausdorff (BCH) formula [62], i.e.,

$$e^{\hat{X}} e^{\hat{Y}} = e^{\hat{Z}} \quad (26)$$

where

$$\hat{Z} = \hat{X} + \hat{Y} + \frac{1}{2} [\hat{X}, \hat{Y}] + \frac{1}{12} [\hat{X}, [\hat{X}, \hat{Y}]] + \dots, \quad (27)$$

to join all the exponential operators in Eq. (23), as we only have to keep the first three terms in the right hand side of Eq. (27) since all the other terms commute. Notice that each time we join two consecutive operators, we get an extra exponential term from the commutation relation in Eq. (25). The exponent of such term adopts the following the form

$$i\varphi_q(t) = -\frac{i}{2} \sum_{i=0}^j \sum_{j=1}^{N-1} \left[\hat{H}_q(t_j), \hat{H}_q(t_i) \right] \Delta t^2 / \hbar^2 \quad (28)$$

and the final time-evolution operator reads

$$\hat{U}_q(t, t_0) = \lim_{N \rightarrow \infty} \exp \left[-i \left(\sum_{i=0}^{N-1} \hat{H}_q(t_i) \right) \Delta t / \hbar \right] e^{i\varphi_q(t)}, \quad (29)$$

where in the exponential operator term we naturally recover the definition of an integral. Thus, according to the definition of $\hat{H}_q(t)$ given in Eq. (20), the previous unitary operator can be written, for the case of the fundamental mode ($q = 1$), as

$$\hat{U}_L(t, t_0) = \exp \left[\delta\alpha_L \hat{a}^\dagger - \delta\alpha_L^* \hat{a} \right] e^{i\varphi_L(t)} \quad (30)$$

which is a displacement in the photonic phase space of a quantity $\delta\alpha_L$ defined by

$$\delta\alpha_L(t) = \mathbf{g}(\omega_L) \cdot \int_{t_0}^t d\tau f(\tau) \mathbf{d}_H(\tau) e^{i\omega_L \tau}. \quad (31)$$

Therefore, incorporating the action of Eq. (29) over the harmonic modes, we finally get the final quantum optical HHG state

$$\begin{aligned} |\Phi(t)\rangle &= e^{i\varphi_L(t)} |(\alpha_L + \delta\alpha_L) e^{-i\omega_L t}\rangle \otimes e^{i\varphi_2(t)} |\beta_2 e^{-i2\omega_L t}\rangle \\ &\quad \otimes \dots \otimes e^{i\varphi_q(t)} |\beta_q e^{-iq\omega_L t}\rangle \otimes \dots, \end{aligned} \quad (32)$$

where we have returned to the original photonic frame of reference, that is, we have undone the initial transformations depicted in Eqs. (5) and (8). Note that here the $i\varphi_q(t)$ are defined as in Eq. (28) once the limit $N \rightarrow \infty$ has been considered. Similarly to the $\delta\alpha_L$, the β_q terms are defined as

$$\beta_q(t) = \sqrt{q} \mathbf{g}(\omega_L) \cdot \int_{t_0}^t d\tau f(\tau) \mathbf{d}_H(\tau) e^{iq\omega_L \tau}. \quad (33)$$

The results obtained until now are valid for the single-atom case. For the N -atomic case, assuming that each atom contributes to the HHG process coherently in a phase matched way, the definitions of $\delta\alpha_L$ and β_q are reformulated as,

$$\delta\alpha_L(t) = N \mathbf{g}(\omega_L) \cdot \int_{t_0}^t d\tau f(\tau) \mathbf{d}_H(\tau) e^{i\omega_L \tau} \quad (34)$$

$$\beta_q(t) = N \sqrt{q} \mathbf{g}(\omega_L) \cdot \int_{t_0}^t d\tau f(\tau) \mathbf{d}_H(\tau) e^{iq\omega_L \tau}. \quad (35)$$

Note that in this case the N -atomic wavefunction will be affected by an overall phase coming from the BCH relation, that does not affect the phase matching conditions which are solely determined by the phase of the generated coherent states. In order to give a physical meaning to $\delta\alpha_L$ and β_q within the electron recollision picture, we will use the Strong Field Approximation theory to provide a solution to the integrals in Eqs. (34) and (35). According to the SFA, it can be shown [26] that the mean value of the dipole operator $\mathbf{d}_H(t)$ reads

$$\begin{aligned} \mathbf{d}_H(t) = & i \int_{t_0}^t dt' \int d\mathbf{v} \mathbf{d}^* \left(\mathbf{p} - \frac{e}{c} \mathbf{A}_L(t') \right) \\ & \times e^{-iS(\mathbf{p}, t, t')} \mathbf{E}_L(t') \\ & \times \mathbf{d} \left(\mathbf{p} - \frac{e}{c} \mathbf{A}_L(t') \right) + \text{c.c.}, \end{aligned} \quad (36)$$

where $\mathbf{A}_L(t)$ is the vector potential of the laser field defined as $\mathbf{E}_L(t) = -(1/c) \partial \mathbf{A}_L(t) / \partial t$, $\mathbf{p} = \mathbf{v} + (e/c) \mathbf{A}_L(t)$ the canonical momentum whereas \mathbf{v} the electron's kinetic momentum, $\mathbf{d}(\mathbf{p} - (e/c) \mathbf{A}_L(t'))$ is the matrix element of the dipole operator between the atomic ground state and the continuum state $|\mathbf{p} - (e/c) \mathbf{A}_L(t')\rangle$, and $S(\mathbf{p}, t, t')$ is the semiclassical action given by

$$S(\mathbf{p}, t, t') = \frac{1}{2} \int_{t'}^t d\tau \left[\mathbf{p} - \frac{e}{c} \mathbf{A}_L(\tau) \right]^2 + I_p(t - t'), \quad (37)$$

where I_p is the ionization potential.

For the sake of simplicity, we will assume that the used laser field consists of a monochromatic field of frequency ω_L , so that we can set $f(t) = 1$ in Eqs. (34) and (35) which now read

$$\delta\alpha_L(t) = N \mathbf{g}(\omega_L) \cdot \int_{t_0}^t d\tau \mathbf{d}_H(\tau) e^{i\omega_L \tau} \quad (38)$$

$$\beta_q(t) = N \sqrt{q} \mathbf{g}(\omega_L) \cdot \int_{t_0}^t d\tau \mathbf{d}_H(\tau) e^{iq\omega_L \tau}. \quad (39)$$

The semiclassical action shown in Eq. (37) is a highly oscillating function which leads to a high oscillating exponent in Eq. (36), and allows for a solution to the triple integration appearing in Eqs. (38), (39) by means of the saddle-point approximation. Therefore, the integrals in Eqs. (38), (39) are completely characterized by the saddle-points determined by the set of variables (\mathbf{p}_s, t_r, t_i) fixed by the following three equations that have been extensively studied in the past within the context of the semiclassical three-step model [7, 26],

$$\frac{[\mathbf{p}_s - \frac{e}{c} \mathbf{A}_L(t_i)]^2}{2} + I_p = 0, \quad (40)$$

$$\int_{t_i}^{t_r} d\tau \left[\mathbf{p}_s - \frac{e}{c} \mathbf{A}_L(\tau) \right] = 0, \quad (41)$$

$$\frac{[\mathbf{p}_s - \frac{e}{c} \mathbf{A}_L(t_r)]^2}{2} + I_p = q\omega_L. \quad (42)$$

In brief terms, the above equations define the three-steps of the recollision process: (40) defines the ionization time t_i , (41) the electron's return to the parent ion, and (42) the recombination time t_r associated with the generation of high harmonics with frequencies $q\omega_L > I_p$. On the one hand, these equations imply that the shift $\delta\alpha_L$ of the coherent state is directly related to the electron ionization and acceleration processes. On the other hand, they also show that the well-known features of the HHG process are transferred to the coherent states of the harmonic field, that is, the β_q 's contain information about the spectral phase and amplitude distribution of the emitted harmonics. In fact, this can be shown by calculating the spectrum of the generated harmonics, which can be obtained from their energy $\langle \hat{H}_f \rangle_{\text{em}} = \sum_q \hbar\omega_q n_q$. In this expression, n_q is the number of photons at frequency $\omega_q = q\omega_L$ which, according to Eq. (35), is given by

$$n_q = N^2 |\mathbf{g}(\omega_q) \cdot \mathbf{d}_H(q\omega_L)|^2. \quad (43)$$

To obtain Eq. (43), we have sent the integration limits to $\pm\infty$, implying that the electric field is introduced at $t_0 = -\infty$ and lasts until $t = +\infty$, so that the integral appearing in Eq. (39) represents the Fourier transform of the mean-valued dipole $\mathbf{d}_H(q\omega_L)$. Considering all possible frequencies, its summation can be rewritten as an integral, and the energy of the emitted harmonics reads

$$E_{\text{em}} = \frac{V_{\text{eff}}}{(2\pi c)^3} \int d\Omega d\omega N^2 \omega^3 |\mathbf{g}(\omega) \cdot \mathbf{d}_H(\omega)|^2, \quad (44)$$

where $d\Omega$ represents the infinitesimal solid angle element. Substituting the definition of $\mathbf{g}(\omega_L)$ into Eq. (44), we find for its integrand

$$\mathcal{E}_{\text{HHG}}(\omega_q) \propto N^2 \omega_q^4 |\mathbf{d}_H(\omega_q)|^2, \quad (45)$$

which corresponds to the expression of the HHG spectrum obtained by the semiclassical theory [7, 26].

1. Effects of the coherent shift onto the coherent state of the laser

To study the back-action of the electron acceleration over the initial state of the system, we investigate the phase space dynamics of $\delta\alpha_L$ using the mean value of the photonic quadratures \hat{x}_L and \hat{p}_L . We furthermore consider the interaction of the laser pulse with a single atom, so that $\delta\alpha_L$ is determined by Eq. (31). Defining \hat{x}_L, \hat{p}_L as

$$\hat{x}_L = \frac{1}{\sqrt{2}} (\hat{a} + \hat{a}^\dagger) \quad \text{and} \quad \hat{p}_L = \frac{1}{i\sqrt{2}} (\hat{a} - \hat{a}^\dagger), \quad (46)$$

it can be shown that their mean values with respect to Eq. (32) are

$$\begin{aligned} \langle \hat{x}_L(t) \rangle &= \sqrt{2} |\alpha_L + \delta\alpha_L(t)| \cos(\omega_L t + \theta(t)) \\ \langle \hat{p}_L(t) \rangle &= -\sqrt{2} |\alpha_L + \delta\alpha_L(t)| \sin(\omega_L t + \theta(t)). \end{aligned} \quad (47)$$

In the previous expressions, $\theta(t)$ is the phase factor of $(\alpha + \delta\alpha_L(t)) = |\alpha + \delta\alpha_L|e^{-i\theta(t)}$. The integral defining $\delta\alpha_L(t)$ was calculated numerically employing $\mathbf{d}_H(t)$ extracted from the QPROP software [63], using a sinusoidal squared laser pulse envelope with 12 cycles and fundamental wavelength $\lambda_L = 800$ nm. The results for these calculations are shown in Fig. 1, where in particular Fig. 1a shows the amplitude shift of the coherent state in phase space, while Fig. 1b shows the time dependence of the amplitude $|\alpha_L + \delta\alpha_L|$ and the phase factor $\theta(t)$ (inset in Fig. 1b).

The dynamics of $\delta\alpha_L$ are summarized in the following four main features: i) during the acceleration process the ionized electron absorbs photons resulting in an enhancement of $|\delta\alpha_L|$, i.e., a reduction of $|\alpha_L + \delta\alpha_L|$; ii) the $|\delta\alpha_L|$ increases with the amplitude of the driving field as the electron gains more kinetic energy; iii) the $|\delta\alpha_L|$ continuously increases during the laser pulse (having a maximum enhancement rate at the peak of the pulse envelope, where the field amplitude is maximum), reaching its maximum value at the end of the pulse; iv) the $|\delta\alpha_L|$ enhancement rate follows the gradient of the driving electric field amplitude. This leads to an oscillatory modulation of frequency $2\omega_L$ of the enhancement of $|\delta\alpha_L|$ during the laser pulse. It is noted that an oscillatory modulation of frequency $2\omega_L$ has been also observed on the phase $\theta(t)$. However, because this phase shift is in the order of 10^{-3} rad, its influence on the state of the field is considered negligible and, thus, it is not further discussed here.

As $\delta\alpha_L$ represents the absorbed part of the driving field that is necessary for generating the harmonic photons, its definition should account for the probability of absorbing n photons during the electron ionization and acceleration processes. To elaborate on this matter, we use $|\delta\alpha(t, t_0)\rangle$ obtained from applying Eq. (30) to the initial vacuum state (within the shifted frame of reference), for defining the probability of absorbing n photons between times t_0 and t

$$P_n(t, t_0) = |\langle n | \delta\alpha_L(t, t_0) \rangle|^2 = \frac{|\delta\alpha_L(t, t_0)|^{2n}}{n!} e^{-|\delta\alpha(t, t_0)|^2}, \quad (48)$$

and we introduce the average probability of absorbing n photons within a cycle of the field that starts at t_0 and finishes at time T as,

$$\tilde{P}_n = \frac{1}{T - t_0} \int_{t_0}^T dt P_n(t, t_0). \quad (49)$$

The numerical results obtained from this calculation are shown in Fig. 2 for three different intensities of the driving field. As we can see, for each of the curves we get a local maximum in the probability which shifts to bigger values of the number of photons n as the intensity of the field increases. This is consistent with the harmonic plateau structure obtained for the HHG spectrum. As the intensity increases the harmonic cutoff becomes bigger and, in consequence, photons of higher frequency are

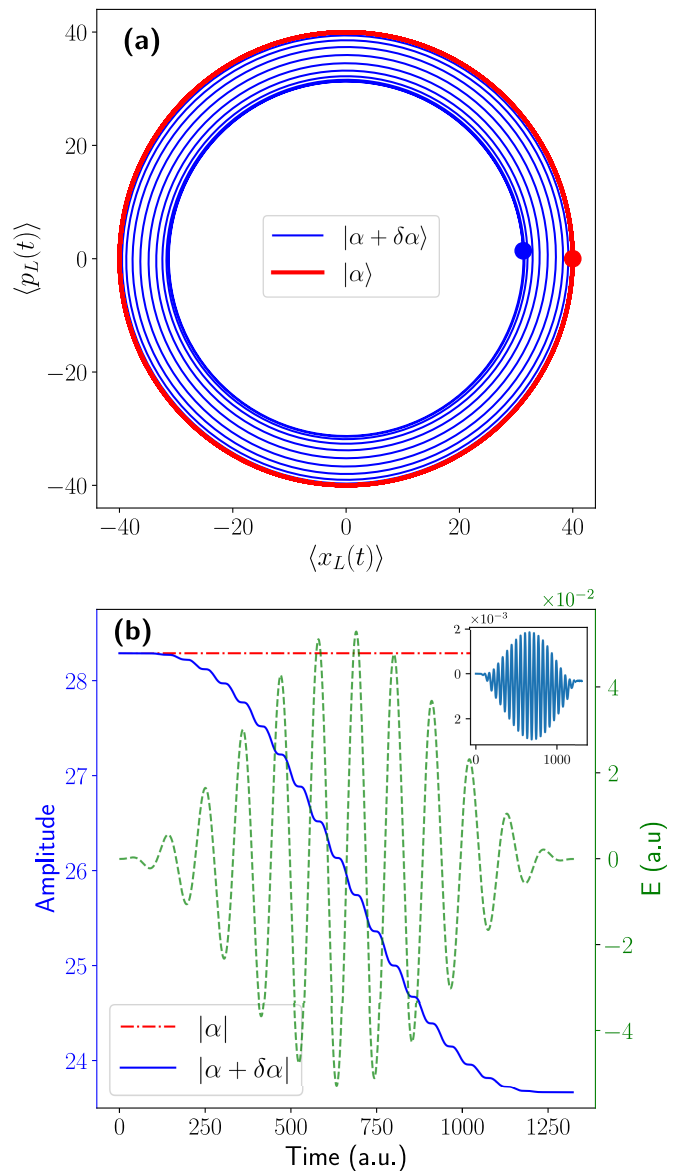


FIG. 1. (a) Dynamics of $|\alpha_L\rangle$ with $|\alpha_L| \approx 28$ (red curve) and $|\alpha_L + \delta\alpha_L(t)\rangle$ (blue curve) in phase space. The analysis was performed using $\mathbf{g}(\omega_L) \approx 10^{-1}$. The red and blue dots depict the final coherent state obtained after the evolution with $|\alpha_L\rangle$ and $|\alpha_L + \delta\alpha_L(t)\rangle$ respectively. (b) Dependence of $|\alpha_L + \delta\alpha_L(t)|$ (blue curve) on time. The red dashed line depicts the initial value of $|\alpha_L|$. The applied electric field is plotted with the dashed green line in atomic units (a.u.). The inset plot represents the dependence of the phase θ with time.

achievable through the HHG process. Thus, given that for generating a photon of frequency $n\omega_L$ a number n of IR photons need to be absorbed, then in order to get a plateau structure for the harmonic spectrum the probability of absorbing IR photons should increase as we move towards the harmonic cutoff, reaching a maximum at this point and decreasing afterwards. To check this, we look at the value of n for which we find a local maximum in the probability (the maximum obtained for $n > 2$) for

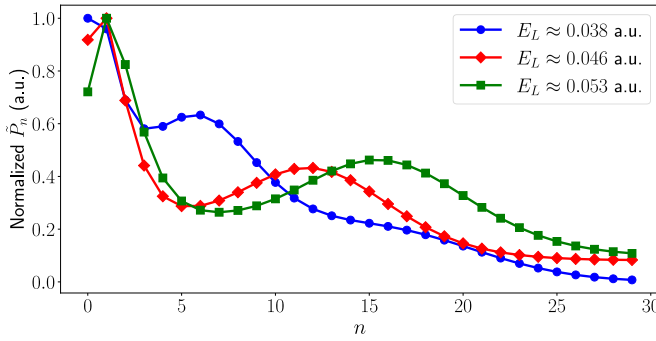


FIG. 2. Normalized average probability of a single atom to absorb n photons for three different electric field amplitudes, $E_L \approx 0.053$ a.u. (green curve), $E_L \approx 0.046$ a.u. (red curve) and $E_L \approx 0.038$ a.u. (blue curve) of the driving field (in atomic units). The results have been obtained by integrating over one cycle of a gaussian shaped pulse with central wavelength $\lambda_L = 800$ nm.

each of the considered intensities. In particular, in Fig. 2 these maxima are placed at $n_{\text{cutoff}} \approx 7, 12$ and 15 from the lowest to the highest intensity respectively, which are in agreement with the cutoffs given by the maximum kinetic energy that an electron can get in the HHG process with the corresponding intensities (the theoretical values for the cutoff are $n_{\text{th}} = 7.71, 11.3$ and 15.0 respectively). Note that in comparison to Eq. (45), here we do not obtain a multi-peak structure involving only the odd harmonics. This is because $\delta\alpha$ describes the amount of IR photons absorbed during the ionization and acceleration processes affecting the fundamental laser mode, which later on will be distributed along the generated harmonics.

2. Creation of optical “kitten” and “cat” states: Conditioning on HHG

In this section we will discuss how the aforementioned results can be used for the creation of non-classical light states in the IR spectral region, in particular Schrödinger “kitten” and “cat” states. Although the above analysis is applicable for high photon numbers, in the following we will discuss the case of low photon number “kitten” and “cat” states. This is because we are interested in providing results that can be used by an experiment that utilizes the Quantum Tomography (QT) method [53, 54] for the quantum state characterization. Thus, as a first step we apply an IR neutral density filter which reduces the amplitude of the fundamental mode mode by a factor of $\cos(r)$. This step is mathematically expressed as,

$$\alpha_L \rightarrow \alpha_L \cos(r) \equiv \alpha \quad \text{and} \quad \delta\alpha_L \rightarrow \delta\alpha_L \cos(r) \equiv \delta\alpha. \quad (50)$$

The key action for creating the non-classical states of light is the post-selection of the coherent shifted state over the part that includes, at least, one harmonic photon. This operation, namely “conditioning on HHG”, can

be mathematically expressed for high values of the harmonic cutoff via the projection operator [64]

$$\hat{P} \approx \mathbb{1} - |\alpha\rangle\langle\alpha|. \quad (51)$$

When this operation acts over the state of the fundamental field after the interaction (final IR state), it leads to the following state

$$|\Phi_{\text{post}}\rangle = \hat{P} |\alpha + \delta\alpha\rangle = |\alpha + \delta\alpha\rangle - \langle\alpha|\alpha + \delta\alpha\rangle |\alpha\rangle, \quad (52)$$

which is basically the superposition of two coherent states, commonly referred to as optical Schrödinger “cat” states [65, 66]. The presence of the tunable $\delta\alpha$ parameter in the superposition allows for the control of the quantum features of the state [67]. For $0 < \langle\alpha + \delta\alpha|\alpha\rangle < 1$ the state is a genuine “cat” which can be switched to a “kitten” when $\langle\alpha + \delta\alpha|\alpha\rangle \rightarrow 1$. In the following we investigate these two cases:

- I) In the limit where the overlap between the original and the shifted coherent state tends to one, i.e., $\langle\alpha + \delta\alpha|\alpha\rangle \rightarrow 1$ so $|\delta\alpha| \rightarrow 0$, we can write our initial state prior to the experimental conditioning up to first order in $|\delta\alpha|$ as (for a more detailed derivation see Appendix A)

$$|\alpha + \delta\alpha\rangle \approx e^{\frac{1}{2}(\alpha^* \delta\alpha - \alpha \delta\alpha^*)} \hat{D}(\alpha) \times (\mathbb{1} + (\delta\alpha \hat{a}^\dagger - \delta\alpha^* \hat{a})) |0\rangle. \quad (53)$$

On the other hand, we have for its projection with respect to $|\alpha\rangle$

$$\langle\alpha|\alpha + \delta\alpha\rangle = e^{\frac{1}{2}(\alpha^* \delta\alpha - \alpha \delta\alpha^*)} e^{-|\delta\alpha|^2/2} \approx e^{\frac{1}{2}(\alpha^* \delta\alpha - \alpha \delta\alpha^*)}, \quad (54)$$

where we have considered again first order terms in $|\delta\alpha|$.

Then, by combining Eqs. (53) and (54) in Eq. (52) we get after normalization

$$|\Phi_{\text{post}}\rangle \approx (\hat{a}^\dagger - \alpha^*) |\alpha\rangle = \hat{D}(\alpha) |1\rangle, \quad (55)$$

which corresponds with the definition of a displaced Fock state, whose photon probability distribution is given by

$$P(n) = \left| \frac{n}{\alpha} - \alpha^* \right|^2 \frac{|\alpha|^{2n}}{n!} e^{-|\alpha|^2} \quad (56)$$

and whose Wigner function [62] is characterized by

$$\begin{aligned} W(\beta) &= \frac{2}{\pi} \text{tr} (\hat{D}(\beta) \hat{\Pi} \hat{D}(-\beta) |\Phi_{\text{post}}\rangle\langle\Phi_{\text{post}}|) \\ &= \frac{2}{\pi} (4|\beta - \alpha|^2 - 1) e^{|\beta - \alpha|^2/2}. \end{aligned} \quad (57)$$

For obtaining this expression, we have used the Wigner function definition of ref. [68], where $\hat{\Pi}$ denotes the parity operator, whose action over the displacement operator is given by $D(-\alpha) = \hat{\Pi} D(\alpha) \hat{\Pi}$.

II) When $0 < \langle \alpha + \delta\alpha | \alpha \rangle < 1$, we obtain a genuine “cat” state (shown in Eq. (52)) with photon number probability distribution

$$P(n) = \frac{1}{N_{\text{cat}}} \left| (\alpha + \delta\alpha)^n e^{-|\alpha + \delta\alpha|^2/2} - \langle \alpha | \alpha + \delta\alpha \rangle \alpha^n e^{-|\alpha|^2/2} \right|^2, \quad (58)$$

and Wigner function

$$W(\beta) = \frac{2}{\pi N_{\text{cat}}} \left[e^{-2|\beta - \alpha - \delta\alpha|^2} + e^{-|\delta\alpha|^2} e^{-2|\beta - \alpha|^2} - (e^{2(\beta - \alpha)\delta\alpha^*} + e^{2(\beta - \alpha)^*\delta\alpha}) e^{-|\delta\alpha|^2} e^{-2|\beta - \alpha|^2} \right], \quad (59)$$

where $N_{\text{cat}} = 1 - e^{-|\delta\alpha|^2}$ is the normalization factor for Eq. (52).

The above cases are shown in Fig. 3, where the Wigner function has been calculated using a 12-cycle sinusoidal pulse of 800 nm wavelength and $E_L = 0.053$ a.u. (corresponding to a laser intensity of about $I = 1 \times 10^{14}$ W/cm²). At the beginning of the pulse, where the amplitude driving field is small, $\delta\alpha$ is small (case I) resulting to the creation of a “kitten” state, while at the end of the pulse where $\delta\alpha$ is getting larger (according to Fig. 1b) the Wigner function depicts a genuine “cat” state (case II). Evidently, in case of reducing the intensity of the driving field the final state would be a “kitten”.

B. Quantum optical description of ATI

As mentioned above, ATI processes happen when the ionized electron either does not re-collide with the parent ion or, if it does, the process takes place elastically. Therefore, to study these phenomena within our formalism, we will condition Eq. (14) upon finding the electron in continuum states, which we will simply represent as $|\mathbf{v}\rangle$, where \mathbf{v} denotes the outgoing kinetic momenta of the electron. Thus, our conditioned Schrödinger equation reads now

$$i\hbar \frac{\partial}{\partial t} \langle \mathbf{v} | \psi(t) \rangle = -\hat{\mathbf{E}}_Q(t) \cdot \langle \mathbf{v} | \mathbf{e} \hat{\mathbf{R}}_H(t) | \psi(t) \rangle. \quad (60)$$

At this point, we introduce SFA theory assumptions [26] and neglect the effects of the electronic bound excited states. Thus, introducing the SFA version of the identity

$$\mathbb{1} \approx |g\rangle\langle g| + \int d\mathbf{v} |\mathbf{v}\rangle\langle \mathbf{v}|, \quad (61)$$

in Eqs. (15) and (60), we get the following set of coupled

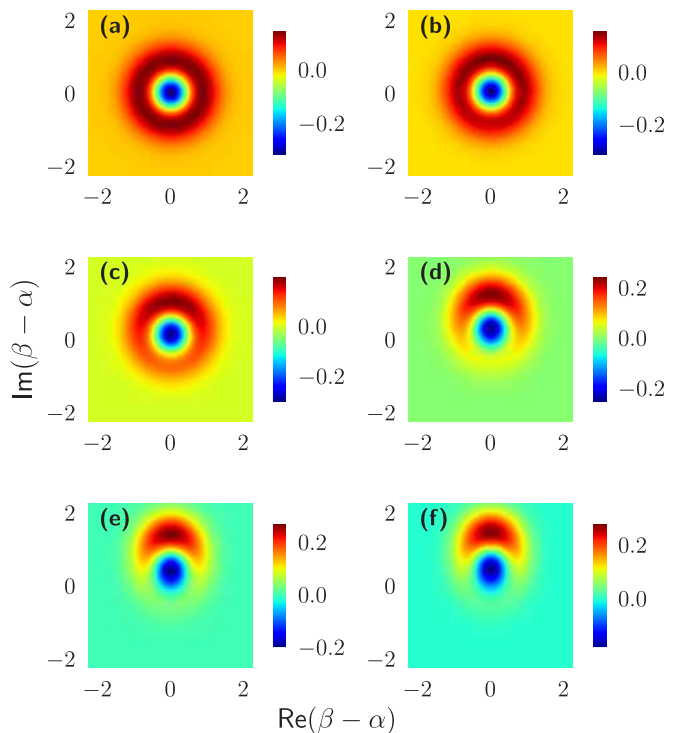


FIG. 3. Dependence of the Wigner function with the amplitude of a multi-cycle and sinusoidal shaped laser pulse with $\omega = 800$ nm after (a) 2, (b) 4, (c) 6, (d) 8, (e) 10 and (f) 12 cycles. $\text{Re}[\beta - \alpha] \equiv x_L, \text{Im}[\beta - \alpha] \equiv p_L$, with x, p the values of the quadrature field operators $\hat{x}_L = (\hat{a} + \hat{a}^\dagger)/\sqrt{2}$ and $\hat{p}_L = (\hat{a} - \hat{a}^\dagger)/i\sqrt{2}$.

differential equations

$$\begin{aligned} i\hbar \frac{\partial}{\partial t} |\Phi(t)\rangle &= -\hat{\mathbf{E}}_Q(t) \cdot \mathbf{d}_H(t) |\Phi(t)\rangle \\ &\quad - \int d\mathbf{v} \hat{\mathbf{E}}_Q(t) \cdot \mathbf{d}_H(\mathbf{v}, t) |\Phi(\mathbf{v}, t)\rangle \\ i\hbar \frac{\partial}{\partial t} |\Phi(\mathbf{v}, t)\rangle &= -\hat{\mathbf{E}}_Q(t) \cdot \mathbf{d}_H^*(\mathbf{v}, t) |\Phi(t)\rangle \\ &\quad - \int d\mathbf{v}' \hat{\mathbf{E}}_Q(t) \cdot \mathbf{d}_H(\mathbf{v}, \mathbf{v}', t) |\Phi(\mathbf{v}', t)\rangle. \end{aligned} \quad (62)$$

Here, we denote the conditioned to ATI state as $|\Phi(\mathbf{v}, t)\rangle = \langle \mathbf{v} | \psi(t) \rangle$ while $\mathbf{d}_H(\mathbf{v}, \mathbf{v}', t) = \langle \mathbf{v} | \mathbf{e} \hat{\mathbf{R}}_H(t) | \mathbf{v}' \rangle$ represents the time-dependent dipole moment matrix element between states $|\mathbf{v}\rangle$ and $|\mathbf{v}'\rangle$.

1. Conditioning with respect to ATI: The first stage

In the first stage of conditioning with the respect to ATI, we must derive the reduced density matrix for the electromagnetic field that corresponds to the ATI process. There are two possible strategies to follow:

I) We can condition on ATI electrons with a specific outgoing direction and kinetic momentum, \mathbf{v} . In

this approach the reduced density matrix of the system is given by,

$$|\Phi(\mathbf{v}, t)\rangle\langle\Phi(\mathbf{v}, t)|, \quad (63)$$

but the experimental detection is clearly tougher: even at fixed kinetic momentum with some error tolerance, there are not so many electrons to detect. We term this case *single-ionization ATI states*.

II) Alternatively, we can condition on all ATI electrons, i.e., consider the reduced density matrix integrated over all outgoing momenta,

$$\int d^3\mathbf{v} |\Phi(\mathbf{v}, t)\rangle\langle\Phi(\mathbf{v}, t)|. \quad (64)$$

Calculations and theoretical description is then more complex, but detection is easier.

In the spirit of the SFA theory, we may neglect the effect of continuum-continuum transitions and obtain the contribution to ATI, corresponding to direct tunnelling, or treat the continuum-continuum transitions perturbatively [69–72] in order to describe re-scattered ATI electrons at higher energies up to $10U_p$, where U_p is the ponderomotive potential defined as $U_p = e^2 E^2 / 4m\omega_L^2$ with E the electric field amplitude and m the electron's mass. In this paper we focus on the latter case, i.e., direct tunneling and electrons of “low” energies $\leq 2U_p$. On the other hand, we keep the same approximations for the first equation as we did in the HHG analysis. With this, we get for the conditioned to ATI state

$$|\Phi(\mathbf{v}, t)\rangle = i\hbar \int_{t_0}^t dt' \hat{\mathbf{E}}_Q(t') \cdot \mathbf{d}_H^*(\mathbf{v}, t') |\Phi(t')\rangle, \quad (65)$$

where $|\Phi(t)\rangle$ is the solution to Eq. (18), that is, the state shown in Eq. (32) before going back to the original frame of reference. Note that \mathbf{v} defines here the kinetic momentum of the outgoing electron.

2. Analysis for single-ionization ATI states

The state shown in Eq. (65) is a superposition of the different coherent shifts generated during the ionization and acceleration processes, each of them multiplied by the matrix element $\mathbf{d}_H^*(\mathbf{v}, t')$, which determines its correlation with the electron's state, associating each shift with the probability amplitude of having a transition from the ground state to the continuum state $|\mathbf{v}\rangle$. However, this state only considers transitions to a particular continuum state.

In this subsection, we are going to consider single-ionization phenomena, i.e., laser ionization phenomena at a given kinetic momentum energy, corresponding to outgoing velocity \mathbf{v} , so that the final ATI quantum state

is indeed well characterized by the pure state given in Eq. (65). Therefore, the obtained results would correspond to an experimental setting where we are able to measure the kinetic energy and direction of the generated photoelectrons, and discard the results whenever the measured kinetic energy and direction are different from those of \mathbf{v} .

In particular, and with the main purpose of obtaining analytical expressions, we will restrict this analysis to time intervals for which the applied strong field is constant, that is, $f(t') = 1$ in Eq. (4) for $t' \in [t_0, t]$. This implies that the amount of photons absorbed every half-cycle of the field would be the same, in opposition to Fig. 1 (b) where the absorption varies every half-cycle due to the modulation of the applied pulse. In practice, this would correspond to a situation where the laser source is a “long” IR pulse, meaning that we can find several cycles with almost the same peak strength on its central part. Thus, and as a first step, we will rewrite Eq. (65) as a sum of integrals defined for every half-cycle of the field

$$|\Phi(\mathbf{v}, t)\rangle = i\hbar \sum_{j=0}^{\mathcal{N}-1} \int_{t_j}^{t_{j+1}} dt' \hat{\mathbf{E}}_Q(t') \cdot \mathbf{d}_H^*(\mathbf{v}, t') \times |\delta\alpha(t')\rangle \bigotimes_{q=2}^{\text{cutoff}} |\beta_q(t')\rangle, \quad (66)$$

where \mathcal{N} is the total number of half-cycles, and we identify $t_{\mathcal{N}} = t$. Note that the conditioning over a single value of direction and kinetic momentum \mathbf{v} leads to an entangled state between all the modes participating in the process. Hereupon, and in order to study the final state obtained for the IR, we will assume that during the ATI process the harmonic coherent state amplitudes β_q stay very close to the vacuum. Thus, if under this assumption we project Eq. (66) over the vacuum state for the harmonics, we can approximate our state by

$$|\tilde{\Phi}(\mathbf{v}, t)\rangle \approx i\hbar \sum_{j=0}^{\mathcal{N}-1} \int_{t_j}^{t_{j+1}} dt' \hat{\mathbf{E}}_L(t') \cdot \mathbf{d}_H^*(\mathbf{v}, t') |\delta\alpha(t')\rangle, \quad (67)$$

where $|\tilde{\Phi}(t)\rangle = \langle 0_q | \bigotimes_q |\Phi(\mathbf{v}, t)\rangle$ and $\hat{\mathbf{E}}_L$ is the electric field operator acting over the fundamental mode, i.e., the first term of Eq. (7).

Furthermore, under the “long” IR pulse considerations, the amount of photons absorbed every half-cycle is the same, that is, $\delta\alpha(t_{j+1}) - \delta\alpha(t_j) = \Delta$. This motivates us to consider a discretization of the values of $\delta\alpha(t)$ appearing on each term of the sum in Eq. (67), such that the value of $\delta\alpha(t)$ in each integral term adopts the value of the coherent state obtained at the end of the cycle, that is,

$$|\tilde{\Phi}(\mathbf{v}, t)\rangle \approx i\hbar \sum_{j=0}^{\mathcal{N}-1} \int_{t_j}^{t_{j+1}} dt' \hat{\mathbf{E}}_L(t') \cdot \mathbf{d}_H^*(\mathbf{v}, t') |(j+1)\Delta\rangle. \quad (68)$$

Of course, this approximation is not always valid. One has to guarantee that two consecutive states $|j\Delta\rangle$ and $|(j+1)\Delta\rangle$ are comparable to each other. Otherwise, smaller steps have to be considered in the discretization, which may not allow us to write the shift Δ as a time-independent quantity. A natural way of establishing such a comparison is in terms of the overlap between these two states, i.e.,

$$\langle j\Delta|(j+1)\Delta\rangle = \exp\left[-\frac{|\Delta|^2}{2}\right]. \quad (69)$$

Thus, we will restrict to values of $|\Delta| < 0.95$, for which the overlap between these two coherent states is bigger than $1 - e^{-1}$. Under these considerations, the state obtained in Eq. (68) is given as a superposition of different coherent states, where each of them is affected by the electric field operator evaluated at time t' . Apart from this, one of the main differences of this state with respect to the one obtained through HHG, in Eq. (52), is that in the former more than two coherent states intervene in the final superposition, depending on the number of half-cycles \mathcal{N} .

In Eq. (68), each of these coherent states is weighted by the quantum optical version of the ATI spectrum taken at every half-cycle of the field. This can be seen more clearly if, assuming a linearly polarized field, we substitute Eq. (4) with the considered approximations in Eq. (68)

$$\begin{aligned} |\phi(\mathbf{v}, t)\rangle &\approx \hbar\mathbf{g}(\omega_L) \\ &\times \sum_{j=0}^{\mathcal{N}-1} \left(\int_{t_j}^{t_{j+1}} dt' \mathbf{d}_H^*(\mathbf{v}, t') e^{i\omega t'} \hat{a} \right. \\ &\quad \left. - \mathbf{d}_H^*(\mathbf{v}, t') e^{-i\omega t'} \hat{a}^\dagger \right) |(j+1)\Delta\rangle, \end{aligned} \quad (70)$$

where

$$\begin{aligned} \mathbf{d}_H^*(\mathbf{v}, t) &= \langle \psi_{\text{sc}}(t) | e^{\hat{X}} U_{\text{sc}}(t) | \mathbf{v} \rangle \\ &= \left\langle \psi_{\text{sc}}(t) \left| e^{\hat{X}} U_{\text{sc}}(t) \left| \mathbf{p} - \frac{e}{c} \mathbf{A}_L(t_0) \right. \right. \right\rangle. \end{aligned} \quad (71)$$

In this last expression \hat{X} is the position coordinate operator affecting the electron, $\hat{U}_{\text{sc}}(t)$ is the time evolution operator of the semiclassical Hamiltonian appearing in Eq. (11), and $|\psi_{\text{sc}}(t)\rangle = U_{\text{sc}}(t) | \mathbf{g} \rangle$ is the ground state of the electron evolved with the previous propagator. Furthermore, we have conditioned over kinetic energies that satisfy $\mathbf{v} = \mathbf{p} - (e/c)\mathbf{A}_L(t_0)$. Under the strong field assumptions, we can write the previous matrix element as

$$\begin{aligned} \mathbf{d}_H^*(\mathbf{v}, t) &= \left\langle \psi_{\text{sc}}(t) \left| e^{\hat{X}} \left| \mathbf{p} - \frac{e}{c} \mathbf{A}_L(t) \right. \right. \right\rangle \\ &\quad \times e^{-i(S(\mathbf{p}, t, t_0) - I_p(t - t_0))}, \end{aligned} \quad (72)$$

with $S(\mathbf{p}, t, t_0)$ the semiclassical action given in Eq. (37). By expanding this expression using the form of $|\psi_{\text{sc}}(t)\rangle$

given by the semiclassical analysis [26], one can see that this term can be written as the sum of two terms characterizing direct ionization phenomena and rescattering processes [73]. In our case, we are only interested in direct ionization processes, so we restrict our calculations to values of the electron kinetic energy lower than $2U_p$, with U_p the ponderomotive potential. Thus, we write this matrix element as

$$\mathbf{d}_H^*(\mathbf{v}, t) \approx \left\langle g \left| e^{\hat{X}} \left| \mathbf{p} - \frac{e}{c} \mathbf{A}_L(t) \right. \right. \right\rangle e^{-i(S(\mathbf{p}, t, t_0) - I_p t)}. \quad (73)$$

In Fig. 4 we present the Wigner functions obtained from Eq. (68) (see Appendix B for its derivation). Their final shape depend mainly on the initial kinetic energy, the number of half-cycles \mathcal{N} , and on the coherent shift Δ obtained in each half-cycle. In our calculations, we assumed that the electron tunnels out to the continuum in a region of maximal intensity of the field, and it does it with zero kinetic energy. On the other hand, the number of cycles is determined by the experimental laser source, and here we consider two cases: a laser source capable of generating $\mathcal{N} = 5$ half cycles of almost equal intensity (Figs. 4 (a) and (b)), and another one generating $\mathcal{N} = 8$ half cycles (Figs. 4 (a) and (b)). Finally, we use $\Delta = 0.25$ (Figs. 4 (a) and (c)) and $\Delta = 0.5$ (Figs. 4 (b) and (d)), satisfying our requirement in Eq. (69). As we can see, for $\mathcal{N} = 5$ half-cycles we get a ring-like shape structure for the Wigner function, quite similar to the one obtained in HHG for small values of $\delta\alpha$ (see Figs. 3 (a) and (b)). This is expected as the distance between the two outermost coherent states appearing in the superposition of Eq. (68), is still small. If we now increase the number of cycles to $\mathcal{N} = 8$, such distance becomes bigger and we find situations like the one in Fig. 4 (d), where we have a very big contribution of a coherent state at $(x = 0, p \approx 4 = \mathcal{N}\Delta)$, and a very small one at $(x = 0, p = 0)$ which are interfering. However, the final distribution differs from the symmetric one coming from an usual coherent state superposition of the form $|\alpha\rangle \pm |-\alpha\rangle$, in that we have more states in the superposition which are contributing as well to the final Wigner function.

3. Analysis for total ATI state

The density matrix that characterizes the total IR ATI state involving all the possible momenta for the generated photoelectrons is

$$\begin{aligned} \rho_{\text{ATI}} &= \int d\mathbf{v} |\Phi(\mathbf{v}, t)\rangle \langle \Phi(\mathbf{v}, t)| \\ &= \int d\mathbf{v} \int_{t_0}^t dt' \int_{t_0}^t dt'' \hat{\mathbf{E}}_Q(t') \cdot \mathbf{d}_H^*(\mathbf{v}, t') \\ &\quad \times |\Phi(t')\rangle \langle \Phi(t'')| \mathbf{d}_H(\mathbf{v}, t'') \cdot \hat{\mathbf{E}}_Q(t''), \end{aligned} \quad (74)$$

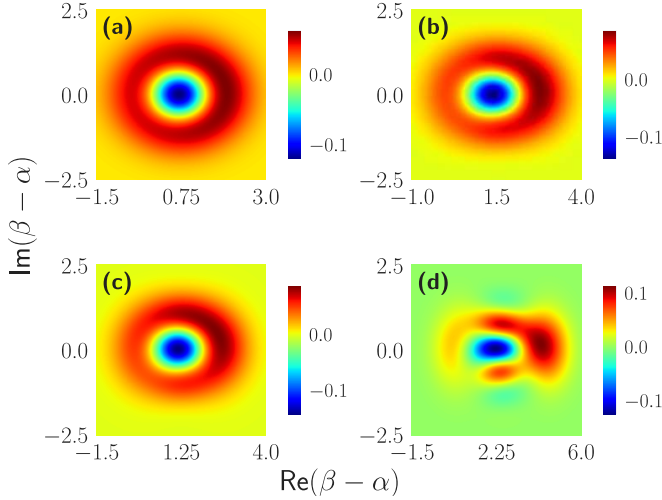


FIG. 4. Dependence of the Wigner function with the number of half-cycles of equal intensity provided by a laser source, and with the shift between two consecutive coherent states Δ . In these subplots we consider: (a) $\mathcal{N} = 5, \Delta = 0.25$; (b) $\mathcal{N} = 5, \Delta = 0.5$; (c) $\mathcal{N} = 8, \Delta = 0.25$; (d) $\mathcal{N} = 8, \Delta = 0.5$. $\text{Re}[\beta - \alpha] \equiv x_L, \text{Im}[\beta - \alpha] \equiv p_L$, with x_L, p_L the values of the quadrature field operators $\hat{x}_L = (\hat{a} + \hat{a}^\dagger)/\sqrt{2}$ and $\hat{p}_L = (\hat{a} - \hat{a}^\dagger)/i\sqrt{2}$.

which, taking into account Eq. (61) and considering for simplicity a linearly polarized light, can be rewritten as

$$\rho_{\text{ATI}} = \int_{t_0}^t dt' \int_{t_0}^t dt'' \hat{E}_Q(t') |\Phi(t')\rangle \langle \Phi(t'')| \hat{E}_Q(t'') \times [\langle \hat{d}_H(t') \hat{d}_H(t'') \rangle - d_H(t') d_H(t'')], \quad (75)$$

where the term between brackets contains the difference between the correlation of the dipole operator at times t' and t'' , and the product of the mean values of such operators at the corresponding times, both terms evaluated with respect to the ground state of the system. For other possible field polarizations, the expression adopts the same form but we would have to consider contributions coming from the different polarization terms for the term between brackets. Obviously, while measurement conditioned on all electrons should be easier, the theoretical analysis is tougher as it requires evaluation of the two-time correlation functions of the dipole moment. This can be done, in principle using SFA or even TDSE, but leads to much more complicated expressions, which will be analysed elsewhere [74].

In order to gain intuition about IR ATI state obtained from Eq. (75), we are going to work within the same approximations that lead to Eq. (67), and considering the simplifying assumption that all the generated coherent shifts are identical and time-independent. In general this is not true and, as discussed in Fig. 1 (b), the coherent shift is continuously increasing along the pulse. However, for single photon ionization processes one may expect this shift to be very small and, in some sense, indistinguishable from all the other values it can take along the whole

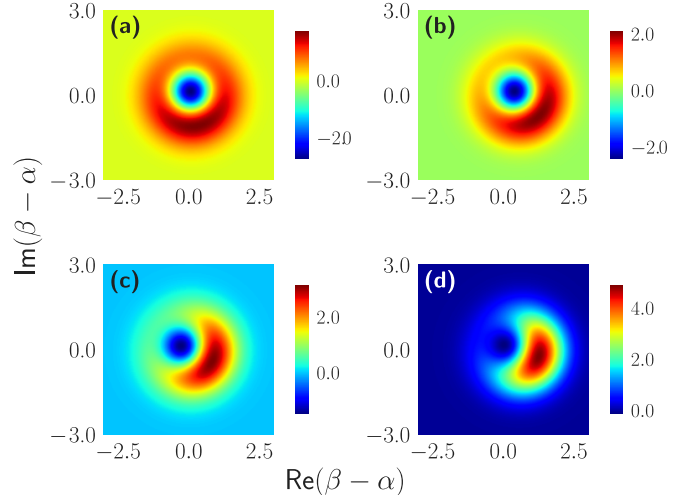


FIG. 5. Calculated non-normalized Wigner functions after considering equal and time-independent coherent-shifts (a) $\delta\alpha = 0.1$, (b) $\delta\alpha = 0.5$, (c) $\delta\alpha = 1$, and (d) $\delta\alpha = 1.5$. For the computation of the Wigner function we have further considered some approximations over their integrals, which are detailed in Appendix C. $\text{Re}[\beta - \alpha] \equiv x_L, \text{Im}[\beta - \alpha] \equiv p_L$, with x_L, p_L the values of the quadrature field operators $\hat{x}_L = (\hat{a} + \hat{a}^\dagger)/\sqrt{2}$ and $\hat{p}_L = (\hat{a} - \hat{a}^\dagger)/i\sqrt{2}$.

pulse duration. Therefore, under this consideration the ATI state reads

$$\tilde{\rho}_{\text{ATI-IR}} = \int_{t_0}^t dt' \int_{t_0}^t dt'' \hat{E}_L(t') |\delta\alpha\rangle \langle \delta\alpha| \hat{E}_L(t'') \times K(t, t'') e^{i\varphi(t)} e^{-i\varphi^*(t'')}, \quad (76)$$

where $K(t, t'') = \langle \hat{d}_H(t') \hat{d}_H(t'') \rangle - d_H(t') d_H(t'')$, and the exponential terms are the factors coming from the BCH formula, which we have to explicitly consider as they cannot be factorized now.

The main advantage of the previous approximation appears when computing the ATI Wigner function

$$W(x, p) = \frac{1}{\pi\hbar} \int_{-\infty}^{\infty} \langle x + y | \tilde{\rho}_{\text{ATI-IR}} | x - y \rangle e^{-i2py/\hbar}, \quad (77)$$

as it can be decomposed as the weighted sum of four terms for which the integrals over y and time become separable (see Appendix C). We also discuss in this appendix some considerations done in the computation of the time-dependent part of such integrals.

The results for the calculated Wigner function are shown in Fig. 5, where in each of the subplots we have considered increasing values of $\delta\alpha$. The structure of the obtained state is very alike to a “cat” state and, as it happens with HHG, as $\delta\alpha$ increases it tends to a typical Gaussian state. Finally, notice that the plots we have presented so far in this section correspond to the state right after the interaction, that is, we have not returned to the laboratory frame of reference as in the HHG characterization. However, this is not a problem as, by imple-

menting them, one finds the same features for the Wigner function upon a shift and a rotation.

III. EXPERIMENTAL RESULTS AND DISCUSSION

The quantum features of the non-classical light state of the fundamental mode exiting the atomic medium depends on the used conditioning approaches (HHG and/or ATI) and on $\delta\alpha$, which introduces the dependence with the gas pressure and the intensity of the driving field in the interaction area (Eq. (34)). Here, the action of conditioning was achieved using the QS approach [51, 55] and the quantum state characterization was performed by means of the well known QT method [53, 54]. In the following, we describe the operation principle of the experimental approach, the dependence of the coherent state superposition (created by conditioning on HHG) on $\delta\alpha$, and the generation of high photon number optical “cat” states.

A. Operation principle of the experimental approach

A block diagram of the experimental approach is shown in Fig. 6a. The setup is divided in four units, where the first concerns the laser beam delivery (LBD) which is used to control the properties of the driving field towards the laser-atom interaction area. It contains the laser beam steering, polarization control, beam shaping, pulse characterization and focusing optics. The second unit is the target area (TA) where the intense laser-atom interaction takes place, and thus where harmonic photons and ATI photoelectrons are generated (left panel in Fig. 6b). It contains the gas medium and the photon/electron detectors. The third, is the attenuation unit which is used to reduce the photon number of the driving field exiting the medium and condition on the HHG/ATI (middle and right panel at Fig. 6b). The fourth unit concerns the QT used for the characterization of the quantum state of light.

An optical layout of the system is shown in Fig. 7. Although the system can be implemented for conditioning on HHG and/or ATI processes, here we will show its applicability using the HHG process induced by the interaction of the fundamental driving field with Xe gas. The operation principle of the system has been extensively discussed in ref. [52]. The experiment was performed using a linearly polarized ≈ 35 fs Ti:Sapphire laser pulse of $\lambda \approx 800$ nm carrier wavelength and an interferometer. The whole system was operating at 0.5 kHz repetition rate. The IR laser beam was separated into the branches of the interferometer by a beam separator BS₁. The reflected by the BS₁ IR beam (in the 2nd branch of the interferometer) serves as a reference beam of the Quantum Tomography method and for measuring (by means of IR

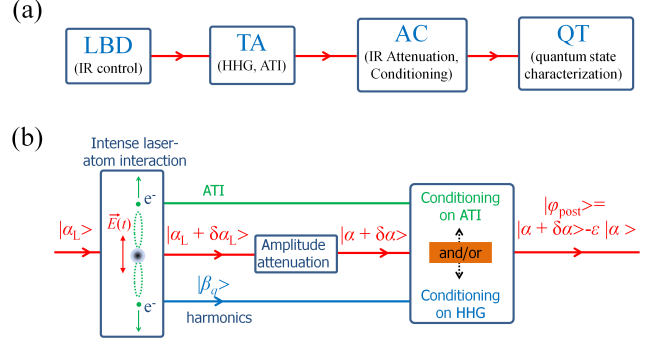


FIG. 6. (a) Block diagram showing the operation principle of the control and characterization of the quantum state of the fundamental light mode exiting the atomic medium. LBD: Laser beam deliver system. TA: Target area. AC: IR attenuation and conditioning unit. QT: Quantum tomography. (b) The left panel is a simplified sketch showing the intense laser-atom interaction in the context of the recollision picture. The middle and right panel shows a schematic of the light attenuation and conditioning on HHG and/or ATI processes, respectively. $|\alpha_L\rangle$ is the coherent state of the driving field, and $|\alpha_L + \delta\alpha_L\rangle$, $|\alpha + \delta\alpha\rangle$, $|\Phi_{\text{post}}\rangle$ are the states of the IR field after the interaction, attenuation and conditioning, respectively, with $\varepsilon = \langle\alpha|\alpha + \delta\alpha\rangle$.

photodiode PD₀) the shot-to-shot energy fluctuations of the driving field. In the 1st branch of the interferometer, the IR beam was focused by means of a 15 cm focal length lens (L₁) into a Xenon pulsed gas jet, where the HHG process takes place. In the present experiment, the optimum intensity of the IR pulse in the interaction region resulting to a maximum harmonic order was $\approx 8 \times 10^{13}$ W/cm², while the maximum harmonic yield was observed for a gas density in the order $\sim 10^{18}$ atoms/cm³. The generated harmonics, after a reflection by a multilayer infrared-antireflection coating plane mirror (HS) placed at grazing incidence angle, was passing through a 150 nm thick Aluminum filter, which selects all the harmonics with $q \geq 11$. The harmonic spectrum, which consists in the harmonics from 11th to 23th with relative amplitudes 0.8:1:0.86:0.52:0.19:0.04:0.02, was measured by means of a conventional XUV-spectrometer (not shown in Fig. 7) and the photon number of the XUV radiation was measured by means of a calibrated XUV detector PD_{HH}. A portion of the IR field exiting the Xenon gas was reflected by the IR beam separator BS₃ towards IR photodiode PD_{out} (placed after a neutral density filter (F) in order to avoid saturation effects). The photocurrent signals i_{HH} , i_0 , i_{out} of PD_{HH}, PD₀ and PD_{out} were used by the QS to disentangle the high harmonic generation process from all other processes induced by the interaction. The IR field after BS₃ was collimated by a concave lens (L₂) while the mean photon number of the IR field (E_{in}), before reaching the balanced detector of the QT, was reduced (by means of neutral density filters F_{in}) to the level of few photons per pulse, with the QS to select, for each laser shot, only the IR photons

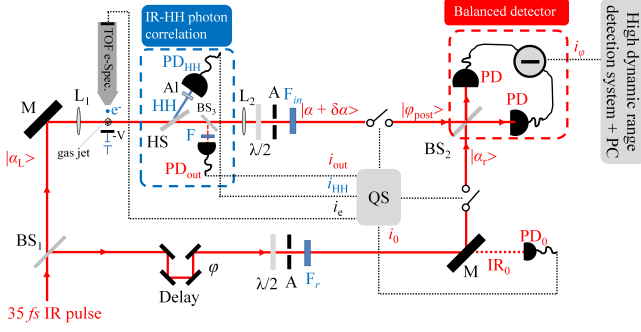


FIG. 7. Experimental arrangement. BS_1 : IR beam separator. $|\alpha_L\rangle$: Coherent state of IR beam passing through BS_1 . $|\alpha_r\rangle$: Coherent state IR beam reflected by BS_1 . M: IR plane mirrors. $L_{1,2}$: Lens. HS: harmonic separator which reflects the high harmonics and leaves the IR beam to pass through. HH: High harmonics. $BS_{2,3}$: IR beam separator and splitter, respectively. PD, PD_0 , PD_{out} , PD_{HH} : IR and HH photodetectors. TOF e-Spec.: μ -metal shielded time of flight spectrometer that could be used for the measurement of the ATI electrons. The voltage (-V) can serve for the energy selection of the electrons reaching the TOF detector. i_ϕ , i_{out} , i_0 , i_{HH} , are the photocurrent values recorded for each laser shot. These were used by the QS in order to condition the $|\alpha_L + \delta\alpha_L\rangle$ state on the HHG process. i_e is the signal of the TOF spectrometer that could be used by QS for conditioning on ATI process. Just before PD_{HH} a 150 nm thick Aluminum filter was placed (not shown) in order to select the harmonics with $q \geq 11$. IR_0 : IR beam used to measure the shot energy of the driving field. $\lambda/2$: Half-IR-wave plates. A: Apertures. $F_{in,r}$: Neutral density filters. $|\alpha + \delta\alpha\rangle$: IR state after the attenuation. All signals were recorded by a high dynamics range boxcar integrator and saved/analyzed by computer (PC) software. $|\Phi_{post}\rangle$ is the quantum state of field entering the balance detector after conditioning on HHG, and E_{in} is the corresponding electric field. $|\alpha_r\rangle$ is the reference coherent state of the laser used by the QT method, and E_r is the corresponding electric field. φ : The controllable phase shift introduced in the reference beam.

related to the HHG. The QS approach [51, 55] relies on shot-to-shot correlation between the photon number of the generated harmonics (integrated signal of $q \geq 11$) and the IR field exiting the medium (gray points in the inset of Fig. 8). The conditioning to HHG is achieved by selecting only the shots that provide signal along the anti-correlation diagonal of the joint distribution (red points in the inset Fig. 8). By selecting these points, we collect only the shots that are relevant to the harmonic emission and we remove the unwanted background associated with all processes irrelevant to the harmonic generation. In this way, we obtain the probability of absorbing IR photons towards the harmonic generation (red line in Fig. 8). The IR absorption probability distribution consists on a multi-peak structure which corresponds to the harmonic order [51, 55]. The black line in Fig. 8 shows the remaining background distribution which needs, and has been subtracted from the data, as is related only with the ability of the present QS experimental apparatus to remove

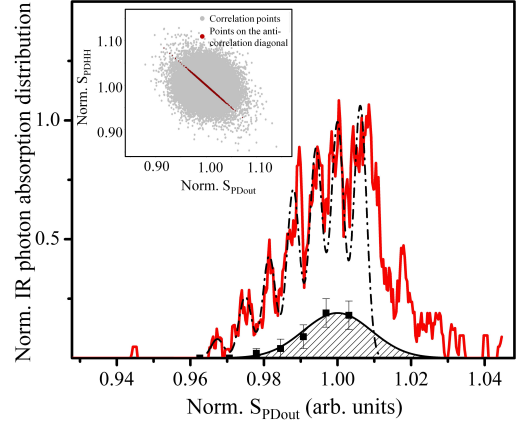


FIG. 8. Probability of absorbing IR photons towards the harmonic generation (red line). The multi-peak structure reflects the spectrum of the emitted harmonics as is described in Sec. II A 2 and refs [51, 52, 55]. The black dashed-dot curve is the best fit of an analytical function given by the sum of a sequence of Gaussian functions. The black shaded area shows the background distribution resulted by fitting a Gaussian function on the data (black squares) obtained by subtracting the minima of the raw data from the minima of the black dashed-dot fit function. The Inset shows the joint XUV-vs-IR photon number distribution using the signal of i_{HH} ($S_{PD_{HH}}$) and i_{out} ($S_{PD_{out}}$) (gray points). The red points show the selected points along the anti-correlation diagonal. The distribution was created by keeping the energy stability of the driving field at the level of $\approx 1\%$, and after subtracting the electronic noise from each laser shot.

all the shots associated with processes irrelevant to the HHG process (for details see refs. [51, 52, 75]).

The E_{in} field was spatiotemporally overlapped on a beam splitter (BS_2) with an unaffected by the interaction local oscillator laser field (E_r) coming from the 2nd branch of the interferometer which consists of a piezo-based delay stage that introduces a controllable delay $\Delta\tau$ (phase shift φ) between the E_r and E_{in} fields. The outgoing from the BS_2 interfering fields were detected by the diodes (PD) of a high bandwidth (from DC to 350 MHz), high subtraction efficiency and high quantum efficiency, balanced amplified differential photodetector, which provides at each value of φ the signal difference. The photocurrent difference i_ϕ , as well as the photocurrent values of the IR and HH detectors (i_{out} , i_0 , i_{HH}) in the QS, were simultaneously recorded for each laser shot by a multichannel 16 bit high dynamic range boxcar integrator. For each shot the background electronic noise was recorded and subtracted by the corresponding photocurrent signal by placing a second time-gate in the boxcar integrator in times significantly delayed compared to the arrival times of the photon signals. Setting the delay stage around $\Delta\tau \approx 0$, the characterization of the quantum state of light was achieved by recording for each shot the value of i_ϕ as a function of φ , by moving the piezo from $\varphi \approx 0$ to $\varphi \approx \pi$. The homodyne data was scaled according to the measured vacuum state quadra-

ture noise.

The values of i_φ used for the characterization of the quantum state are those corresponding to the shots lying along the anti-correlation diagonal. These are directly proportional to the measurement of the electric field operator $\hat{E}_c(\varphi) \propto \hat{x}_\varphi = \cos(\varphi)\hat{x} + \sin(\varphi)\hat{p}$. Repeated measurements of \hat{x}_φ at each φ provides the probability distribution $P_\varphi(x_\varphi) = \langle x_\varphi | \hat{\rho} | x_\varphi \rangle$ of its eigenvalues x_φ (where $\hat{\rho} \equiv |\Phi_{\text{post}}\rangle\langle\Phi_{\text{post}}|$ is the density operator of the light state and $|x_\varphi\rangle$ the eigenstate with eigenvalue x_φ). For each data set in the range of $0 < \varphi < \pi$ around $\Delta\tau \approx 0$, the Wigner function was reconstructed by means of the inverse Radon transformation implemented via the standard filtered back-projection algorithm [53, 54]. The algorithm used to reconstruct the Wigner functions was applied directly to the quadrature values $x_{\varphi,k}$, where k is the index of each value, using the formula [53, 54] $W(x,p) \simeq \frac{1}{2\pi^2 N} \sum_{k=1}^N K(x \cdot \cos(\varphi_k) + p \cdot \sin(\varphi_k) - x_{\varphi,k})$. $K(z) = \frac{1}{2} \int_{-\infty}^{\infty} |\xi| \exp(i\xi z) d\xi$ is called integration kernel with $z = x \cdot \cos(\varphi_k) + p \cdot \sin(\varphi_k) - x_{\varphi,k}$. The numerical implementation of the integration kernel requires the replacement of the infinite integration limits with a finite cutoff frequency k_c . In order to reduce the numerical artifacts (rapid oscillations) and allow the details of the Wigner function to be resolved, the value of k_c was set to ≈ 4.7 for all measurements presented here. An estimation of the error of the reconstructed $W(x,p)$ has been obtained by comparing (subtracting) the ideal Wigner function of a coherent state from the Wigner function of a coherent state reconstructed by the experimental data. The deviation from the ideal case provides an error of ± 0.004 in $W(x,p)$. The accuracy of measuring the photon number was in the range of $\approx 2\%$ to $\approx 4\%$ of the mean, for high and low photon numbers, respectively. This was obtained following the aforementioned procedure using the density matrices ρ_{nm} in Fock space (n, m) . The mean photon number was obtained by the diagonal elements ρ_{nn} of the ρ_{nm} and the relation $\langle n \rangle = \sum n \rho_{nn}$.

B. Dependence of the coherent state superposition on $\delta\alpha$: Optical “kitten” and “cat” states

To show the dependence of the quantum features of the coherent state superposition on $\delta\alpha$, we have measured the $W(x,p)$ for two different values of $\delta\alpha$ when we condition on HHG. This is shown in Fig. 9 together with the measurement of the coherent state of the driving field (Fig. 9a). The left panels show the measured \hat{x}_φ , the middle panels the corresponding reconstructed $W(x,p)$, and the right panels the theoretically calculated $W_{th}(x,p)$. As $\delta\alpha \propto N$ (Eq. (34)), the change of $\delta\alpha$ was achieved by varying the number of atoms N in the interaction region (using the delay between the laser pulse arrival and the opening of the Xe gas nozzle). It is noted that for experimental reasons (gas load in the vacuum chamber), in the present experiment the maximum value of the used N was set such that the harmonic signal was slightly lower

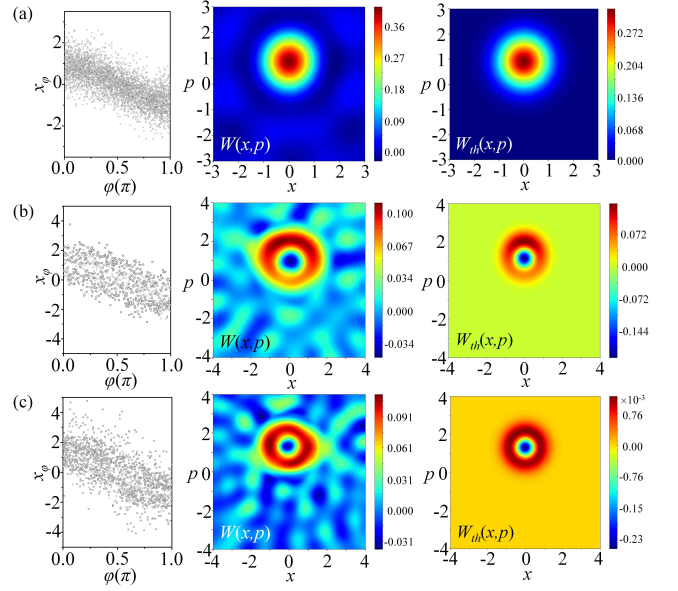


FIG. 9. Optical “cat” and “kitten” states created by conditioning on HHG, for different values of $|\delta\alpha|$. The left, middle and right panels show the measured \hat{x}_φ , the corresponding reconstructed $W(x,p)$, and the theoretically calculated $W_{th}(x,p)$, respectively, projected on (x,p) plane. (a) Coherent state of driving laser field measured when the Xe gas and QS approach were switched-off. (b) Optical “cat” state measured when the Xe gas jet and the QS were switched-on and the harmonic yield was close to maximum. The corresponding $W_{th}(x,p)$ has been calculated for $|\delta\alpha| \approx 0.5$, where $|\alpha| \approx 1.4$ and $|\varepsilon| \approx 0.88$. (c) Optical “kitten” state measured when the the harmonic yield was reduced by a factor of ≈ 25 , i.e., $\delta\alpha$ by a factor of ≈ 5 , compared to the harmonic yield of (b). The corresponding $W_{th}(x,p)$ has been calculated for $|\delta\alpha| \approx 0.1$, where $|\alpha| \approx 1.3$ and $|\varepsilon| \approx 0.99$. x and p are the values of the quadrature field operators $\hat{x} = (\hat{a} + \hat{a}^\dagger)/\sqrt{2}$ and $\hat{p} = (\hat{a} - \hat{a}^\dagger)/i\sqrt{2}$.

(a factor of ≈ 2) than its maximum value. Since the harmonic yield (Y) is $Y \propto N^2$, we then get $\delta\alpha \propto Y^{1/2}$. This relation provides a useful experimental guide for controlling the value of $\delta\alpha$ by monitoring the integrated signal of the harmonics passing through the Aluminum filter.

For reasons of completeness and for evaluating the performance of the experimental setup, it is useful to measure first the coherent state of the driving field by switching-off the Xe gas jet and the QS. This is shown in Fig. 9a. As expected, the state of the IR driving field is coherent, depicting a $W(x,p)$ with Gaussian distribution. The same result was obtained when the Xe gas and the QS were switched on and off, respectively. By switching-on both, the Xe gas jet (at conditions where the harmonic generation yield is close to maximum) and the QS, as reported in ref [52], an optical “cat” state with $\langle n \rangle \approx 1.74 \pm 0.03$ has been recorded (Fig. 9b). The $W(x,p)$ depicts a half-ring-like shape with a central negative minimum located at $(x_{min}, p_{min}) \approx (0, 1)$ and a maximum at $(x_{max}, p_{max}) \approx (0, 2)$, which is in agreement to the $W_{th}(x,p)$ obtained by the theoretical calcu-

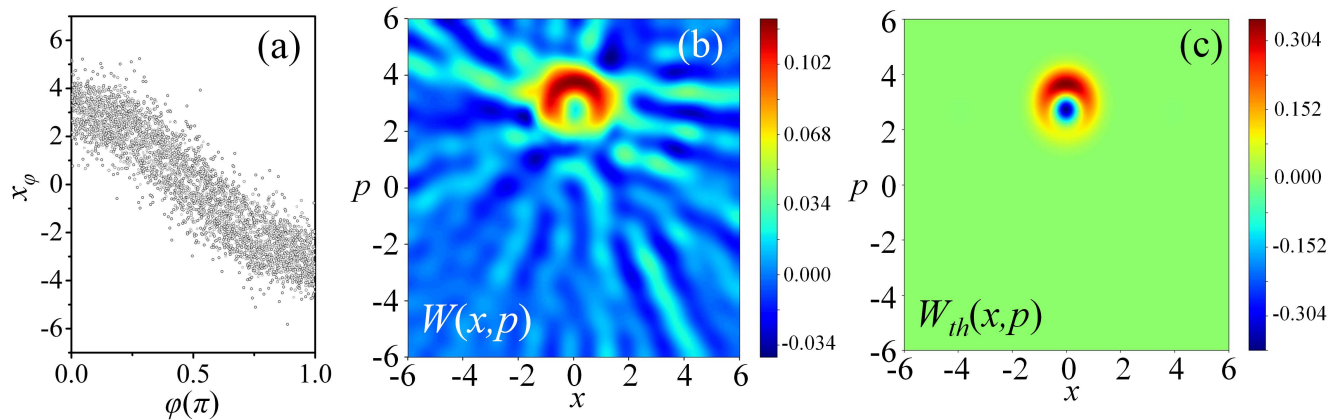


FIG. 10. High photon number optical “cat” state created by conditioning on HHG. (a) Measured \hat{x}_φ with Xenon gas and QS switched-on. (b) Projection on (x, p) plane of the reconstructed $W(x, p)$ which shows an optical “cat” state of $\langle n \rangle \approx 9.4 \pm 0.1$. (c) Theoretically calculated Wigner function $W_{th}(x, p)$ for $|\delta\alpha| \approx 0.8$, where $|\alpha| \approx 3.7$ and $|\varepsilon| \approx 0.73$. x and p are the values of the quadrature field operators $\hat{x} = (\hat{a} + \hat{a}^\dagger)/\sqrt{2}$ and $\hat{p} = (\hat{a} - \hat{a}^\dagger)/i\sqrt{2}$.

lations for $|\delta\alpha|$ in the range of 0.4 to 0.5. In Fig. 9b we show the $W_{th}(x, p)$ for $|\delta\alpha| \approx 0.5$, where $|\alpha| \approx 1.4$ and $|\varepsilon| \equiv |\langle \alpha + \delta\alpha | \alpha \rangle| \approx 0.88$. The value of $|\alpha|$ has been obtained by the equation $\langle n \rangle = \langle \Phi_{\text{post}} | \hat{n} | \Phi_{\text{post}} \rangle$ using as $\langle n \rangle$ the value of the measured mean photon number. When we reduce the Y by a factor of ≈ 25 , i.e., $\delta\alpha$ by a factor of ≈ 5 , the state superposition transitions from an optical “cat” to “kitten” state. This is shown in Fig. 9c where an optical “kitten” state with $\langle n \rangle \approx 2.54 \pm 0.05$ has been recorded. In this case, the measured $W(x, p)$ depicts a full-ring shape with a central negative minimum located at $(x_{min}, p_{min}) \approx (0, 1.2)$. This is in agreement with the $W_{th}(x, p)$ obtained by the theoretical calculations obtained for $|\delta\alpha| \approx 0.1$, where $|\alpha| \approx 1.3$ and $|\varepsilon| \approx 0.99$. We note that for values of $|\delta\alpha| < 0.1$, our cat state behaves as a displaced Fock state, as there are no pronounced maximum on the ring shape phase space distribution.

C. Generation of high photon number optical “cat” states

For applications in quantum technology it is also important to be able to increase the photon number of the produced optical “cat” states. As was mentioned before, the present approach can be used for the production of arbitrary high photon number “cat” states. To show this, we have recorded a 9-photon optical “cat” state (Fig. 10) created by conditioning on HHG. Fig. 10a shows the measurement of \hat{x}_φ used to reconstruct the Wigner function shown in phase space in Fig. 10b. The measurement was performed using a value of N approximately close to the value used to record the low photon number optical “cat” state shown in Fig. 9b, while the photon number has been increased by means of F_{in} (Fig. 7). In this case, an optical “cat” state with $\langle n \rangle \approx 9.4 \pm 0.1$ has been recorded. The $W(x, p)$ depicts a half-ring-like shape with a cen-

tral minimum located at $(x_{min}, p_{min}) \approx (0, 2.8)$ and a maximum at $(x_{max}, p_{max}) \approx (0, 3.7)$. The shape of the measured $W(x, p)$ is reasonably close to the Wigner function ($W_{th}(x, p)$) obtained by the theoretical calculations for $|\delta\alpha|$ in the range of 0.6 to 1.1. In Fig. 10c we show the $W_{th}(x, p)$ for $|\delta\alpha| \approx 0.8$, where $|\alpha| \approx 3.7$ and $|\varepsilon| \approx 0.73$. The lack of negative values at the position of the minimum of the measured $W(x, p)$, is attributed to limitations of the present experimental approach in obtaining the Wigner function and the photon number with accuracy better than ± 0.004 and $\approx 2\%$, respectively.

IV. CONCLUSIONS

In this work, we investigated the quantum optics of strongly laser driven atoms. Using a fully quantized theoretical approach, we described the HHG and ATI processes and we showed how the conditioning on HHG and ATI processes can naturally lead to the generation of amplitude-shifted coherent state superpositions. Additionally, we have investigated the parameters that can be used to control the quantum features of these states. This was experimentally confirmed by measuring the quantum features of the coherent state superposition obtained after conditioning on HHG for different gas densities. We found that the coherent state superposition transitions from an optical “cat” to “kitten” state as the number of atoms participating in the harmonic generation process is reduced. We also show that the procedure can be used for the generation of high photon number coherent state superpositions. This has been experimentally confirmed by recording a 9-photon optical “cat” state. Finally, considering that the strong field laser-atom interaction is at the core of strong laser field physics, it can be considered that the work builds the basis for the development of a new class of non-classical light sources and for in-

vestigations on quantum optics, exploiting interactions induced in matter using laser intensities in the moderate and relativistic regions [75].

Acknowledgments

We thank Jens Biegert, Ido Kaminer and Pascal Salières for enlightening discussions. We also thank I. Liontos, E. Skantzakis from FORTH and S. Karsch from Max Planck Institute for Quantum Optics for his assistance on maintaining the performance of the Ti:Sa laser system.

ICFO group acknowledges support from ERC AdG NOQIA, State Research Agency AEI (“Severo Ochoa” Center of Excellence CEX2019-000910-S, Plan National FIDEUA PID2019-106901GB-I00/10.13039 / 501100011033, FPI, QUANTERA MAQS PCI2019-111828-2 / 10.13039/501100011033), RETOS-QUSPIN, Fundació Privada Cellex, Fundació Mir-Puig, Generalitat de Catalunya (AGAUR Grant No. 2017 SGR 1341, CERCA program, QuantumCAT U16-011424, co-funded by ERDF Operational Program of Catalonia 2014-2020), EU Horizon 2020 FET-OPEN OPTOLogic (Grant No 899794), and the National Science Centre, Poland (Symfonia Grant No. 2016/20/W/ST4/00314), Marie Skłodowska-Curie grant STREDCH No 101029393, “La Caixa” Junior Leaders fellowships (ID100010434), and EU Horizon 2020 under Marie Skłodowska-Curie grant agreement No 847648 (LCF/BQ/PI19/11690013, LCF/BQ/PI20/11760031, LCF/BQ/PR20/11770012).

J.R.-D. acknowledges support from the Secretaria d’Universitats i Recerca del Departament d’Empresa i Coneixement de la Generalitat de Catalunya, as well as the European Social Fund (L’FSE inverteix en el teu futur)–FEDER.

P.T. group acknowledges LASERLABEUROPE (H2020-EU.1.4.1.2 grant no.654148), FORTH Synergy Grant AgiIDA (grand no. 00133), the H2020 framework program for research and innovation under the NFFA-Europe-Pilot project (grand no. 101007417). ELI-ALPS is supported by the European Union and co-financed by the European Regional Development Fund (GINOP Grant No. 2.3.6-15-2015-00001).

References

- [1] A. McPherson, G. Gibson, H. Jara, U. Johann, T. S. Luk, I. A. McIntyre, K. Boyer, and C. K. Rhodes, Studies of multiphoton production of vacuum-ultraviolet radiation in the rare gases, *JOSA B* **4**, 595 (1987).
- [2] M. Ferray, A. L’Huillier, X. F. Li, L. A. Lompre, G. Mainfray, and C. Manus, Multiple-harmonic conversion of 1064 nm radiation in rare gases, *Journal of Physics B: Atomic, Molecular and Optical Physics* **21**, L31 (1988).
- [3] M. Lewenstein and A. L’Huillier, Principles of Single Atom Physics: High-Order Harmonic Generation, Above-Threshold Ionization and Non-Sequential Ionization, in *Strong Field Laser Physics*, Springer Series in Optical Sciences, edited by T. Brabec (Springer, New York, NY, 2009) pp. 147–183.
- [4] J.-F. Hergott, M. Kovacev, H. Merdji, C. Hubert, Y. Mairesse, E. Jean, P. Breger, P. Agostini, B. Carré, and P. Salières, Extreme-ultraviolet high-order harmonic pulses in the microjoule range, *Physical Review A* **66**, 021801 (2002).
- [5] E. Constant, D. Garzella, P. Breger, E. Mével, C. Dorrer, C. Le Blanc, F. Salin, and P. Agostini, Optimizing High Harmonic Generation in Absorbing Gases: Model and Experiment, *Physical Review Letters* **82**, 1668 (1999).
- [6] C. M. Heyl, C. L. Arnold, A. Couairon, and A. L’Huillier, Introduction to macroscopic power scaling principles for high-order harmonic generation, *Journal of Physics B: Atomic, Molecular and Optical Physics* **50**, 013001 (2016).
- [7] K. Amini, J. Biegert, F. Calegari, A. Chacón, M. F. Ciappina, A. Dauphin, D. K. Efimov, C. F. d. M. Faria, K. Giergiel, P. Gniewek, A. S. Landsman, M. Lesiuk, M. Mandrysz, A. S. Maxwell, R. Moszyński, L. Ortmann, J. A. Pérez-Hernández, A. Picón, E. Pisanty, J. Prauzner-Bechcicki, K. Sacha, N. Suárez, A. Zaïr, J. Zakrzewski, and M. Lewenstein, Symphony on strong field approximation, *Reports on Progress in Physics* **82**, 116001 (2019).
- [8] S. M. Teichmann, F. Silva, S. L. Cousin, M. Hemmer, and J. Biegert, 0.5-keV Soft X-ray attosecond continua, *Nature Communications* **7**, 11493 (2016).
- [9] D. Popmintchev, B. R. Galloway, M.-C. Chen, F. Dollar, C. A. Mancuso, A. Hankla, L. Miaja-Avila, G. O’Neil, J. M. Shaw, G. Fan, S. Ališauskas, G. Andriukaitis, T. Balčiunas, O. D. Mücke, A. Pugzlys, A. Baltuška, H. C. Kapteyn, T. Popmintchev, and M. M. Murnane, Near- and Extended-Edge X-Ray-Absorption Fine-Structure Spectroscopy Using Ultrafast Coherent High-Order Harmonic Supercontinua, *Physical Review Letters* **120**, 093002 (2018).
- [10] F. Krausz and M. Ivanov, Attosecond physics, *Reviews of Modern Physics* **81**, 163 (2009).
- [11] M. F. Ciappina, J. A. Pérez-Hernández, A. S. Landsman, W. A. Okell, S. Zherebtsov, B. Förg, J. Schötz, L. Seifert, T. Fennel, T. Shaaran, T. Zimmermann, A. Chacón, R. Guichard, A. Zaïr, J. W. G. Tisch, J. P. Marangos, T. Witting, A. Braun, S. A. Maier, L. Roso, M. Krüger, P. Hommelhoff, M. F. Kling, F. Krausz, and M. Lewenstein, Attosecond physics at the nanoscale, *Reports on Progress in Physics* **80**, 054401 (2017).
- [12] Y. Kobayashi, T. Sekikawa, Y. Nabekawa, and S. Watanabe, 27-fs extreme ultraviolet pulse generation by high-order harmonics, *Optics Letters* **23**, 64 (1998).
- [13] K. Midorikawa, Y. Nabekawa, and A. Suda, XUV multiphoton processes with intense high-order harmonics, *Progress in Quantum Electronics* **32**, 43 (2008).
- [14] S. Chatziathanasiou, S. Kahaly, E. Skantzakis, G. Sansone, R. Lopez-Martens, S. Haessler, K. Varju, G. D. Tsakiris, D. Charalambidis, and P. Tzallas, Generation of Attosecond Light Pulses from Gas and Solid State Media, *Photonics* **4**, 26 (2017).
- [15] N. Tsatrafyllis, B. Bergues, H. Schröder, L. Veisz, E. Skantzakis, D. Gray, B. Bodi, S. Kuhn, G. D. Tsakiris, D. Charalambidis, and P. Tzallas, The ion microscope as a tool for quantitative measurements in the extreme ultraviolet, *Scientific Reports* **6**, 21556 (2016).

- [16] B. Bergues, D. E. Rivas, M. Weidman, A. A. Muschet, W. Helml, A. Guggenmos, V. Pervak, U. Kleineberg, G. Marcus, R. Kienberger, D. Charalambidis, P. Tzallas, H. Schröder, F. Krausz, and L. Veisz, Tabletop nonlinear optics in the 100-eV spectral region, *Optica* **5**, 237 (2018).
- [17] A. Nayak, I. Orfanos, I. Makos, M. Dumergue, S. Kühn, E. Skantzakis, B. Bodi, K. Varju, C. Kalpouzos, H. I. B. Banks, A. Emmanouilidou, D. Charalambidis, and P. Tzallas, Multiple ionization of argon via multi-XUV-photon absorption induced by 20-GW high-order harmonic laser pulses, *Physical Review A* **98**, 023426 (2018).
- [18] B. Senfftleben, M. Kretschmar, A. Hoffmann, M. Sauppe, J. Tümmeler, I. Will, T. Nagy, M. J. J. Vrakking, D. Rupp, and B. Schütte, Highly non-linear ionization of atoms induced by intense high-harmonic pulses, *Journal of Physics: Photonics* **2**, 034001 (2020).
- [19] I. Orfanos, I. Makos, I. Lontos, E. Skantzakis, B. Major, A. Nayak, M. Dumergue, S. Kühn, S. Kahaly, K. Varju, G. Sansone, B. Witzel, C. Kalpouzos, L. A. A. Nikolopoulos, P. Tzallas, and D. Charalambidis, Non-linear processes in the extreme ultraviolet, *Journal of Physics: Photonics* **2**, 042003 (2020).
- [20] C. Gohle, T. Udem, M. Herrmann, J. Rauschenberger, R. Holzwarth, H. A. Schuessler, F. Krausz, and T. W. Hänsch, A frequency comb in the extreme ultraviolet, *Nature* **436**, 234 (2005).
- [21] A. Cingöz, D. C. Yost, T. K. Allison, A. Ruehl, M. E. Fermann, I. Hartl, and J. Ye, Direct frequency comb spectroscopy in the extreme ultraviolet, *Nature* **482**, 68 (2012).
- [22] L. Young, K. Ueda, M. Gühr, P. H. Bucksbaum, M. Simon, S. Mukamel, N. Rohringer, K. C. Prince, C. Masciovecchio, M. Meyer, A. Rudenko, D. Rolles, C. Bostedt, M. Fuchs, D. A. Reis, R. Santra, H. Kapteyn, M. Murnane, H. Ibrahim, F. Légaré, M. Vrakking, M. Isinger, D. Kroon, M. Gisselbrecht, A. L'Huillier, H. J. Wörner, and S. R. Leone, Roadmap of ultrafast x-ray atomic and molecular physics, *Journal of Physics B: Atomic, Molecular and Optical Physics* **51**, 032003 (2018).
- [23] S. Fuchs, M. Wünsche, J. Nathanael, J. J. Abel, C. Rödel, J. Biedermann, J. Reinhard, U. Hübner, and G. G. Paulus, Optical coherence tomography with nanoscale axial resolution using a laser-driven high-harmonic source, *Optica* **4**, 903 (2017).
- [24] P. B. Corkum, Plasma perspective on strong field multiphoton ionization, *Physical Review Letters* **71**, 1994 (1993).
- [25] K. C. Kulander, K. J. Schafer, and J. L. Krause, Dynamics of Short-Pulse Excitation, Ionization and Harmonic Conversion, in *Super-Intense Laser-Atom Physics*, NATO ASI Series, edited by B. Piraux, A. L'Huillier, and K. Rzażewski (Springer US, Boston, MA, 1993) pp. 95–110.
- [26] M. Lewenstein, P. Balcou, M. Y. Ivanov, A. L'Huillier, and P. B. Corkum, Theory of high-harmonic generation by low-frequency laser fields, *Physical Review A* **49**, 2117 (1994).
- [27] G. G. Paulus, W. Nicklich, H. Xu, P. Lambropoulos, and H. Walther, Plateau in above threshold ionization spectra, *Physical Review Letters* **72**, 2851 (1994).
- [28] R. J. Glauber, Nobel Lecture: One hundred years of light quanta, *Reviews of Modern Physics* **78**, 1267 (2006).
- [29] A. Acín, I. Bloch, H. Buhman, T. Calarco, C. Eichler, J. Eisert, D. Esteve, N. Gisin, S. J. Glaser, F. Jelezko, S. Kuhr, M. Lewenstein, M. F. Riedel, P. O. Schmidt, R. Thew, A. Wallraff, I. Walmsley, and F. K. Wilhelm, The quantum technologies roadmap: a European community view, *New Journal of Physics* **20**, 080201 (2018).
- [30] I. A. Walmsley, Quantum optics: Science and technology in a new light, *Science* **348**, 525 (2015).
- [31] S. Mukamel, M. Freyberger, W. Schleich, M. Bellini, A. Zavatta, G. Leuchs, C. Silberhorn, R. W. Boyd, L. L. Sánchez-Soto, A. Stefanov, M. Barbieri, A. Paterova, L. Krivitsky, S. Shwartz, K. Tamasaku, K. Dorfman, F. Schlawin, V. Sandoghdar, M. Raymer, A. Marcus, O. Varnavski, T. Goodson, Z.-Y. Zhou, B.-S. Shi, S. Asban, M. Scully, G. Agarwal, T. Peng, A. V. Sokolov, Z.-D. Zhang, M. S. Zubairy, I. A. Vartanyants, E. d. Valle, and F. Laussy, Roadmap on quantum light spectroscopy, *Journal of Physics B: Atomic, Molecular and Optical Physics* **53**, 072002 (2020).
- [32] I. H. Deutsch, Harnessing the Power of the Second Quantum Revolution, *PRX Quantum* **1**, 020101 (2020).
- [33] G. Mourou, Nobel Lecture: Extreme light physics and application, *Reviews of Modern Physics* **91**, 030501 (2019).
- [34] D. Strickland, Nobel Lecture: Generating high-intensity ultrashort optical pulses, *Reviews of Modern Physics* **91**, 030502 (2019).
- [35] K. J. LaGattuta, Radiation emitted by a resonantly driven hydrogen atom, *Physical Review A* **48**, 666 (1993).
- [36] B. Wang, Y. Guo, J. Chen, Z.-C. Yan, and P. Fu, Frequency-domain theory of nonsequential double ionization in intense laser fields based on nonperturbative QED, *Physical Review A* **85**, 023402 (2012).
- [37] D. N. Yangaliev, V. P. Krainov, and O. I. Tolstikhin, Quantum theory of radiation by nonstationary systems with application to high-order harmonic generation, *Physical Review A* **101**, 013410 (2020).
- [38] F. I. Gauthey, C. H. Keitel, P. L. Knight, and A. Maquet, Role of initial coherence in the generation of harmonics and sidebands from a strongly driven two-level atom, *Physical Review A* **52**, 525 (1995).
- [39] Á. Gombkötő, S. Varró, P. Mati and P. Földi, High-order harmonic generation as induced by a quantized field: Phase-space picture, *Physical Review A* **101**, 013418 (2020).
- [40] Á. Gombkötő, A. Czirják, Attila, S. Varró and P. Földi, Quantum-optical model for the dynamics of high-order-harmonic generation, *Physical Review A* **94**, 013853 (2016).
- [41] J. Gao, F. Shen, and J. G. Eden, Interpretation of high-order harmonic generation in terms of transitions between quantum Volkov states, *Physical Review A* **61**, 043812 (2000).
- [42] P. Fu, B. Wang, X. Li, and L. Gao, Interrelation between high-order harmonic generation and above-threshold ionization, *Physical Review A* **64**, 063401 (2001).
- [43] H. Hu and J. Yuan, Time-dependent QED model for high-order harmonic generation in ultrashort intense laser pulses, *Physical Review A* **78**, 063826 (2008).
- [44] M. Y. Kuchiev and V. N. Ostrovsky, Quantum theory of high-harmonic generation via above-threshold ionization and stimulated recombination, *Journal of Physics B: Atomic, Molecular and Optical Physics* **32**, L189 (1999).

- [45] V. I. Usachenko and V. A. Pazdersky, High-order harmonic generation in a strong laser field: an alternative quantum-mechanical model, *Journal of Physics B: Atomic, Molecular and Optical Physics* **35**, 761 (2002).
- [46] A. V. Bogatskaya, E. A. Volkova, and A. M. Popov, Spontaneous emission of atoms in a strong laser field, *Journal of Experimental and Theoretical Physics* **125**, 587 (2017).
- [47] I. A. Burenkov and O. V. Tikhonova, Features of multiphoton-stimulated bremsstrahlung in a quantized field, *Journal of Physics B: Atomic, Molecular and Optical Physics* **43**, 235401 (2010).
- [48] A. Gorlach, O. Neufeld, N. Rivera, O. Cohen, and I. Kaminer, The quantum-optical nature of high harmonic generation, *Nature Communications* **11**, 4598 (2020).
- [49] Á. Gombkötő, P. Földi, and S. Varró, Quantum-optical description of photon statistics and cross correlations in high-order harmonic generation, *Phys. Rev. A* **104**, 033703 (2021).
- [50] I. A. Gonoskov, N. Tsatrafyllis, I. K. Kominis, and P. Tzallas, Quantum optical signatures in strong-field laser physics: Infrared photon counting in high-order-harmonic generation, *Scientific Reports* **6**, 32821 (2016).
- [51] N. Tsatrafyllis, I. K. Kominis, I. A. Gonoskov, and P. Tzallas, High-order harmonics measured by the photon statistics of the infrared driving-field exiting the atomic medium, *Nature Communications* **8**, 15170 (2017).
- [52] M. Lewenstein, M. F. Ciappina, E. Pisanty, J. Rivera-Dean, P. Stammer, T. Lamprou, and P. Tzallas, Generation of optical schrödinger cat states in intense laser-matter interactions, *Nat. Phys.* (2021).
- [53] G. Breitenbach, S. Schiller, and J. Mlynek, Measurement of the quantum states of squeezed light, *Nature* **387**, 471 (1997).
- [54] A. I. Lvovsky and M. G. Raymer, Continuous-variable optical quantum-state tomography, *Reviews of Modern Physics* **81**, 299 (2009).
- [55] N. Tsatrafyllis, S. Kühn, M. Dumergue, P. Foldi, S. Kahaly, E. Cormier, I. Gonoskov, B. Kiss, K. Varju, S. Varro, and P. Tzallas, Quantum Optical Signatures in a Strong Laser Pulse after Interaction with Semiconductors, *Physical Review Letters* **122**, 193602 (2019).
- [56] J. Rivera-Dean, T. Lamprou, E. Pisanty, P. Stammer, A. F. Ordóñez, M. F. Ciappina, M. Lewenstein, and P. Tzallas, Quantum optics of strongly laser-driven atoms and generation of high photon number optical cat states, Zenodo 10.5281/zenodo.5524648 (2021).
- [57] A. Wünsche, Quantization of Gauss–Hermite and Gauss–Laguerre beams in free space, *Journal of Optics B: Quantum and Semiclassical Optics* **6**, S47 (2004).
- [58] G. Grynberg, A. Aspect, and C. Fabre, *Introduction to Quantum Optics: From the Semi-classical Approach to Quantized Light* (Cambridge University Press, Cambridge, 2010).
- [59] W. Vogel and D.-G. Welsch, *Quantum Optics* (John Wiley & Sons, 2006).
- [60] T. Schultz and M. Vrakking, *Attosecond and XUV Physics: Ultrafast Dynamics and Spectroscopy* (John Wiley & Sons, 2014).
- [61] J. Tannor, David, *Introduction to Quantum Mechanics: A Time-Dependent Perspective* (University Science Books, 2007).
- [62] W. P. Schleich, *Quantum Optics in Phase Space* (John Wiley & Sons, 2011).
- [63] D. Bauer and P. Koval, Qprop: A Schrödinger-solver for intense laser–atom interaction, *Computer Physics Communications* **174**, 396 (2006).
- [64] P. Stammer, J. Rivera-Dean, T. Lamprou, E. Pisanty, M. F. Ciappina, P. Tzallas, and M. Lewenstein, High photon number entangled states and coherent state superposition from the extreme-ultraviolet to the far infrared, arXiv:2107.12887 [physics, physics:quant-ph] (2021), arXiv: 2107.12887.
- [65] M. Brune, S. Haroche, J. M. Raimond, L. Davidovich, and N. Zagury, Manipulation of photons in a cavity by dispersive atom-field coupling: Quantum-nondemolition measurements and generation of “Schrödinger cat” states, *Physical Review A* **45**, 5193 (1992).
- [66] S. Deléglise, I. Dotsenko, C. Sayrin, J. Bernu, M. Brune, J.-M. Raimond, and S. Haroche, Reconstruction of non-classical cavity field states with snapshots of their decoherence, *Nature* **455**, 510 (2008).
- [67] J. Rivera-Dean, P. Stammer, E. Pisanty, T. Lamprou, P. Tzallas, M. Lewenstein, and M. F. Ciappina, New schemes for creating large optical Schrodinger cat states using strong laser fields, arXiv:2107.12811 [physics, physics:quant-ph] (2021).
- [68] A. Royer, Wigner function as the expectation value of a parity operator, *Physical Review A* **15**, 449 (1977).
- [69] M. Lewenstein, K. C. Kulander, K. J. Schafer, and P. H. Bucksbaum, Rings in above-threshold ionization: A quasiclassical analysis, *Phys. Rev. A* **51**, 1495 (1995).
- [70] N. Suárez, A. Chacón, M. F. Ciappina, J. Biegert, and M. Lewenstein, Above-threshold ionization and photoelectron spectra in atomic systems driven by strong laser fields, *Phys. Rev. A* **92**, 063421 (2015).
- [71] N. Suárez, A. Chacón, M. F. Ciappina, B. Wolter, J. Biegert, and M. Lewenstein, Above-threshold ionization and laser-induced electron diffraction in diatomic molecules, *Phys. Rev. A* **94**, 043423 (2016).
- [72] N. Suárez, A. Chacón, E. Pisanty, L. Ortmann, A. S. Landsman, A. Picón, J. Biegert, M. Lewenstein, and M. F. Ciappina, Above-threshold ionization in multicenter molecules: The role of the initial state, *Phys. Rev. A* **97**, 033415 (2018).
- [73] D. B. Milošević, G. G. Paulus, D. Bauer, and W. Becker, Above-threshold ionization by few-cycle pulses, *Journal of Physics B: Atomic, Molecular and Optical Physics* **39**, R203 (2006).
- [74] P. Stammer, J. Rivera-Dean, T. Lamprou, M. F. Ciappina, A. S. Maxwell, A. F. Ordóñez, E. Pisanty, P. Tzallas, and M. Lewenstein, in preparation (2021).
- [75] T. Lamprou, R. Lopez-Martens, S. Haessler, I. Lontos, S. Kahaly, J. Rivera-Dean, P. Stammer, E. Pisanty, M. F. Ciappina, M. Lewenstein, and P. Tzallas, Quantum-Optical Spectrometry in Relativistic Laser–Plasma Interactions Using the High-Harmonic Generation Process: A Proposal, *Photonics* **8**, 192 (2021).

A. Detailed derivation of the kitten state

As mentioned in the text, the kitten state is obtained in the limit where $\langle \alpha | \alpha + \delta \alpha \rangle \rightarrow 1$ which corresponds to the limit where $|\delta \alpha| \rightarrow 0$. This is valid whenever $\delta \alpha$ adds a depletion to the initial coherent state, a condition that is verified when the phase of $\delta \alpha$ and α , which we denote

here as θ_δ and θ_α respectively, satisfy

$$\frac{\pi}{2} + \arcsin\left(\frac{|\delta\alpha|}{2|\alpha|}\right) + \theta_\alpha < \theta_\delta < \frac{3\pi}{2} - \arcsin\left(\frac{|\delta\alpha|}{2|\alpha|}\right) + \theta_\alpha. \quad (\text{A1})$$

In order to work in regimes of vanishing $|\delta\alpha|$, we will consider an expansion of the postprocessed state presented in Eq. (52) in terms of powers of $|\delta\alpha|$. With that purpose, we first write our shifted coherent state $|\alpha + \delta\alpha\rangle$ as

$$|\alpha + \delta\alpha\rangle = \hat{D}(\alpha)e^{\frac{1}{2}(\alpha^*\delta\alpha - \alpha\delta\alpha^*)}\hat{D}(\delta\alpha)|0\rangle, \quad (\text{A2})$$

where we have considered the following property of the displacement operator

$$\hat{D}(\alpha + \delta\alpha) = e^{\frac{1}{2}(\alpha^*\delta\alpha - \alpha\delta\alpha^*)}\hat{D}(\alpha)\hat{D}(\delta\alpha). \quad (\text{A3})$$

Introducing here the definition of the displacement operator $D(\alpha)$ and in particular its polynomial expansion

$$\begin{aligned} \hat{D}(\delta\alpha) &= \exp[\delta\alpha\hat{a}^\dagger - \delta\alpha^*\hat{a}] = \sum_{n=0}^{\infty} \frac{(\delta\alpha\hat{a}^\dagger - \delta\alpha^*\hat{a})^n}{n!} \\ &= \sum_{n=0}^{\infty} |\delta\alpha|^n \frac{(e^{i\theta_\delta}\hat{a}^\dagger - e^{-i\theta_\delta}\hat{a})^n}{n!}, \end{aligned} \quad (\text{A4})$$

which, introduced in Eq. (A2), leads to the desired polynomial expansion in $|\delta\alpha|$

$$\begin{aligned} |\alpha + \delta\alpha\rangle &= \hat{D}(\alpha)e^{\frac{1}{2}(\alpha^*\delta\alpha - \alpha\delta\alpha^*)} \\ &\times \sum_{n=0}^{\infty} |\delta\alpha|^n \frac{(e^{i\theta_\delta}\hat{a}^\dagger - e^{-i\theta_\delta}\hat{a})^n}{n!} |0\rangle, \end{aligned} \quad (\text{A5})$$

and whose scalar product with $|\alpha\rangle$ is given by

$$\begin{aligned} \langle\alpha|\alpha + \delta\alpha\rangle &= e^{\frac{1}{2}(\alpha^*\delta\alpha - \alpha\delta\alpha^*)} \langle 0|\delta\alpha\rangle \\ &= e^{\frac{1}{2}(\alpha^*\delta\alpha - \alpha\delta\alpha^*)} e^{-|\delta\alpha|^2/2} \\ &= e^{\frac{1}{2}(\alpha^*\delta\alpha - \alpha\delta\alpha^*)} \sum_{n=0}^{\infty} \frac{1}{2^n} \frac{|\delta\alpha|^{2n}}{n!}. \end{aligned} \quad (\text{A6})$$

Combining Eqs. (A5) and (A6) with Eq. (52) we then get

$$\begin{aligned} |\Phi_{\text{post}}\rangle &= e^{\frac{1}{2}(\alpha^*\delta\alpha - \alpha\delta\alpha^*)}\hat{D}(\alpha) \\ &\times \sum_{n=1}^{\infty} \left(|\delta\alpha|^n \frac{(e^{i\theta_\delta}\hat{a}^\dagger - e^{-i\theta_\delta}\hat{a})^n}{n!} - \frac{1}{2^n} \frac{|\delta\alpha|^{2n}}{n!} \right) |0\rangle, \end{aligned} \quad (\text{A7})$$

where we start the sum at $n = 1$ because the $n = 0$ term cancels due to the equal contribution of the two terms in the difference. Thus, the previous difference leads to

$$|\Phi_{\text{post}}\rangle = e^{\frac{1}{2}(\alpha^*\delta\alpha - \alpha\delta\alpha^*)}\hat{D}(\alpha)\left(\delta\alpha\hat{a}^\dagger|0\rangle + \mathcal{O}(|\delta\alpha|^2)\right), \quad (\text{A8})$$

which up to first order in $|\delta\alpha|$ corresponds with the definition of a displaced Fock state.

B. ATI Wigner function for single-ionization ATI states

Here, we explicitly compute the expression for the Wigner function of the state in Eq. (68). With that purpose, let us first define the quantities A_j and B_j as

$$\begin{aligned} A_j &= \hbar\mathbf{g}(\omega_L) \int_{t_j}^{t_{j+1}} dt' \mathbf{d}_H^*(\mathbf{v}, t') e^{i\omega t'} \\ B_j &= \hbar\mathbf{g}(\omega_L) \int_{t_j}^{t_{j+1}} dt' \mathbf{d}_H^*(\mathbf{v}, t') e^{-i\omega t'}, \end{aligned} \quad (\text{B1})$$

where $\mathbf{d}_H^*(\mathbf{v}, t)$ is given as in Eq. (73), such that the state in Eq. (68) can be written as

$$|\tilde{\Phi}(\mathbf{v}, t)\rangle = i \sum_{j=0}^{\mathcal{N}-1} (A_j\hat{a} - B_j\hat{a}^\dagger) |(j+1)\Delta\rangle. \quad (\text{B2})$$

Introducing here the definition of the photonic quadrature operators, \hat{x}_L and \hat{p}_L , given in Eq. (46), we can rewrite the previous state as

$$|\tilde{\Phi}(\mathbf{v}, t)\rangle = i \sum_{j=0}^{\mathcal{N}-1} (C_j^{(-)}\hat{x}_L + iC_j^{(+)}\hat{p}_L) |(j+1)\Delta\rangle, \quad (\text{B3})$$

where $C_j^\pm = (1/\sqrt{2})(A_j \pm B_j)$. Thus, for computing the Wigner function by means of Eq. (77), we first give an expression for the matrix element of $\rho = |\tilde{\Phi}(\mathbf{v}, t)\rangle\langle\tilde{\Phi}(\mathbf{v}, t)|$ between two different position states $|x \pm y\rangle$

$$\begin{aligned} \langle x + y|\rho|x - y\rangle &= \left[\sum_{j=0}^{\mathcal{N}-1} C_j^{(+)} \langle x + y|\hat{x}_L|(j+1)\Delta\rangle \right. \\ &\quad \left. + iC_j^{(-)} \langle x + y|\hat{p}_L|(j+1)\Delta\rangle \right] \\ &\times \left[\sum_{k=0}^{\mathcal{N}-1} C_k^{(+)*} \langle (k+1)\Delta|\hat{x}_L|x - y\rangle \right. \\ &\quad \left. - iC_k^{(-)*} \langle (k+1)\Delta|\hat{p}_L|x - y\rangle \right], \end{aligned} \quad (\text{B4})$$

with

$$\begin{aligned} \langle x + y|\hat{x}_L|(j+1)\Delta\rangle &= (x + y)G_{+,j} \\ \langle x + y|\hat{p}_L|(j+1)\Delta\rangle &= -i \frac{\partial G_{+,j}}{\partial(x + y)}, \end{aligned} \quad (\text{B5})$$

where the functions $G_{\pm,j} = \langle x \pm y|(j+1)\Delta\rangle$ are given by

$$\langle x|\alpha\rangle = \frac{1}{\pi^{1/4}} \exp\left[-\frac{(x - \sqrt{2}\text{Re}(\alpha))^2}{2} + ix\sqrt{2}\text{Im}(\alpha)\right]. \quad (\text{B6})$$

With all this, the matrix element in Eq. (B4) reads

$$\begin{aligned} \langle x+y|\rho|x-y\rangle &= \sum_{j,k}^{\mathcal{N}-1} \left[C_j^{(-)} C_k^{(-)*} (x^2 - y^2) G_{+,j} G_{-,k}^* \right. \\ &\quad + C_j^{(+)} C_k^{(+)*} \frac{\partial G_{+,j}}{\partial(x+y)} \frac{\partial G_{-,k}^*}{\partial(x-y)} \\ &\quad + C_j^{(-)} C_k^{(+)*} (x+y) G_{+,j} \frac{\partial G_{-,k}^*}{\partial(x-y)} \\ &\quad \left. + C_j^{(+)} C_k^{(-)*} (x-y) \frac{\partial G_{+,j}}{\partial(x+y)} G_{-,k}^* \right], \end{aligned} \quad (\text{B7})$$

and, thus, the Wigner function can be computed by introducing this expression for the matrix element inside Eq. (77). Note that this expression will only contain derivatives involving Gaussian functions, so it can be computed analytically. In particular, we have performed these calculations in atomic units ($\hbar = 1, e^2 = 1, m_e = 1$ and $k_c = 1/4\pi\epsilon_0 = 1$). In particular, we considered the ionization potential of an hydrogen atom $I_p = 0.5$ a.u., the frequency for the fundamental mode $\omega = 0.057$ a.u., and the amplitude of the electromagnetic field $E_L = 0.053$ a.u..

C. ATI Wigner function for the constant coherent shift analysis

In this appendix we explicitly compute the Wigner function for the ATI density matrix under the assumption considered in the main text, that is, with generated coherent shift being a constant. As shown in Eq. (77), for its evaluation we first need to compute $\langle x+y|\tilde{\rho}_{\text{ATI-IR}}|x-y\rangle$, which is given by

$$\begin{aligned} \langle x+y|\tilde{\rho}_{\text{ATI-IR}}|x-y\rangle &= \\ &\int_0^t dt' \int_0^{t'} dt'' \langle x+y|\hat{E}_Q(t')|\delta\alpha\rangle \langle \delta\alpha|\hat{E}_Q(t'')|x-y\rangle \\ &\quad \times K(t, t'') e^{\phi(t)} e^{\phi^*(t'')}. \end{aligned} \quad (\text{C1})$$

With the purpose of evaluating the matrix elements between the position states $|x \pm y\rangle$ and the coherent state $|\delta\alpha\rangle$, we write the electric field operator defined in Eq. (7) (considering only the fundamental mode) as

$$\hat{E}_Q(t) = \sqrt{2}g(\omega_L)f(t)[\hat{x}_L \sin(\omega_L t) - \hat{p}_L \cos(\omega_L t)], \quad (\text{C2})$$

where we have used the definition of the creation and annihilation operators in terms of the quadrature operators (see Eq. (46)), and working in atomic units. With this, we get for the considered matrix elements

$$\begin{aligned} \langle x \pm y|\hat{E}_Q(t)|\alpha\rangle &= \sqrt{2}g(\omega_L)f(t) \\ &\quad \times \left[(x \pm y)G_{\pm} \sin(\omega_L t) + i \frac{\partial G_{\pm}}{\partial(x \pm y)} \cos(\omega_L t) \right], \end{aligned} \quad (\text{C3})$$

where, we denote $G_{\pm} = \langle x \pm y|\delta\alpha\rangle$.

By introducing Eq. (C3) into Eq. (C1) and after working out a little bit the obtained expression, we get that the Wigner function can be written as

$$W = \frac{2g(\omega_L)}{\pi^2} (W_1 + W_2 - iW_3 + iW_4), \quad (\text{C4})$$

where each of these terms is defined as follows

$$\begin{aligned} W_1 &= \left(\int_{-\infty}^{\infty} dy (x^2 - y^2) G_+ G_-^* e^{-i2py/\hbar} \right) \\ &\quad \left(\int_0^T dt \int_0^T dt' K(t, t') e^{\varphi(t)} e^{\varphi^*(t')} \sin(\omega_L t) \sin(\omega_L t') \right), \end{aligned} \quad (\text{C5})$$

$$\begin{aligned} W_2 &= \left(\int_{-\infty}^{\infty} dy \frac{\partial G_+}{\partial(x+y)} \frac{\partial G_-^*}{\partial(x-y)} e^{-i2py/\hbar} \right) \\ &\quad \left(\int_0^T dt \int_0^T dt' K(t, t') e^{\varphi(t)} e^{\varphi^*(t')} \cos(\omega_L t) \cos(\omega_L t') \right), \end{aligned} \quad (\text{C6})$$

$$\begin{aligned} W_3 &= \left(\int_{-\infty}^{\infty} dy (x+y) G_+ \frac{\partial G_-^*}{\partial(x-y)} e^{-i2py/\hbar} \right) \\ &\quad \left(\int_0^T dt \int_0^T dt' K(t, t') e^{\varphi(t)} e^{\varphi^*(t')} \sin(\omega_L t) \cos(\omega_L t') \right), \end{aligned} \quad (\text{C7})$$

$$\begin{aligned} W_4 &= \left(\int_{-\infty}^{\infty} dy (x-y) G_-^* \frac{\partial G_+}{\partial(x+y)} e^{-i2py/\hbar} \right) \\ &\quad \left(\int_0^T dt \int_0^T dt' K(t, t') e^{\varphi(t)} e^{\varphi^*(t')} \cos(\omega_L t) \sin(\omega_L t') \right). \end{aligned} \quad (\text{C8})$$

One of the main problems with respect to these integrals is the time-dependent part, as it depends on the correlator $K(t, t')$. This is something that cannot be computed naturally through TDSE, neither through SFA. For that reason, and in order to have a rough idea of what can we expect from the ATI processes, we considered all the time-dependent integrals to have the same order of magnitude, which is a fair assumption as all of them present the same dependence. Nevertheless, slight variations to Fig. (5) are obtained depending on the different relative weights between these terms, all of them giving rise to the same final overall structure of the obtained states.